Chemotherapy-driven *de novo* Wnt pathway activation dictates a dynamic shift to a drug-tolerant state in breast cancer cells

Youssef El Laithy[1], Willy Antoni Abreu De Oliveira[1], Anirudh Pabba[2], Alessandra Qualizza[1], François Richard[2], Paraskevi Athanasouli[1], Carla Rios Luci[3], Wout De Wispelaere[4], Larissa Mourao[5], Siân Hamer[6], Stijn Moens[4], Anchel De Jaime-Soguero[1], Maria Francesca Baietti[7], Stefan J Hutten[8,9], Jos Jonkers[8,9], Stephen-John Sammut[10,11], Stefaan Soenen[3], Colinda LGJ Scheele[5], Alejandra Bruna[6], Christine Desmedt[2], Daniela Annibali[4], Frederic Lluis[1*].

[1] Stem Cell Institute, Department of Development and Regeneration, Katholieke Universiteit (KU) Leuven, Leuven, 3000, Belgium.
[2] Laboratory for Translational Breast Cancer Research, Department of Oncology, KU Leuven, Leuven, 3000 Belgium.
[3] NanoHealth and Optical Imaging Group, Department of Imaging & Pathology, KU Leuven, Leuven, 3000, Belgium.
[4] Gynecological Oncology, Department of Oncology, KU Leuven, Leuven, 3000, Belgium.
[5] Laboratory of Intravital Microscopy and Dynamics of Tumor Progression, Department of Oncology, VIB-KU Leuven Center for Cancer Biology, Leuven, 3000, Belgium.
[6] Preclinical Modelling of Pediatric Cancer Evolution, Institute of Cancer Research (ICR), London, SM2 5NG, United Kingdom.
[7] TRACE – Laboratory for RNA Cancer Biology, Department of Oncology, KU Leuven, Leuven, 3000 Belgium.
[8] Division of Molecular Pathology, The Netherlands Cancer Institute, Amsterdam, 1066CX, The Netherlands.
[9] Oncode Institute, Amsterdam, 1066CX, The Netherlands.
[10] Breast Cancer Now Toby Robins Research Center, Institute of Cancer Research (ICR), London, SM2 5NG, United Kingdom.
[11] The Royal Marsden Hospital, NHS Foundation Trust, London, SW3 6JJ, United Kingdom.

* Correspondence to: Frederic Lluis – frederic.lluisvinas@kuleuven.be

ABSTRACT

The efficacy of chemotherapy is often hindered by the enrichment of drug-tolerant persister (DTP) cells, which are known to drive therapy resistance. Unraveling and targeting the early events leading to therapy-induced DTP cell-enrichment presents a potential avenue for innovative therapeutic strategies. In this study, we identified the activation of the Wnt/β-catenin signaling pathway as a common mechanism underlying early DTP cell-enrichment in response to different chemotherapeutic agents in Triple-negative breast cancer (TNBC). Live-imaging reveals *de novo* transcriptional Wnt-activation prevailing over intrinsic selection post chemotherapy. Importantly, Wnt-active (Wnt^{High}) cells exhibit transcriptional and functional similarities to DTP cells, such as a diapause transcriptional signature, reduced proliferation, and marked chemoresistance. The transition to a post-treatment Wnt^{High} state is driven by increased expression of key components involved in canonical Wnt ligand-secretion and -activation. Genetic interference or concomitant, rather than sequential, pharmacologic inhibition of Wnt ligand-secretion alongside chemotherapy prevents treatment-induced Wnt^{High} enrichment, sensitizing TNBC tumors to chemotherapy. This study enhances our understanding of the introductory mechanisms driving DTP cell-enrichment upon chemotherapy.

42 **INTRODUCTION**

43 Systemic cytotoxic chemotherapy, employing different drugs such as taxanes, anthracyclines, or platinum-
44 based salts, is one of the most widely accepted treatment modalities for malignant tumors, including
45 triple-negative breast cancer (TNBC)[1–3]. Many patients with TNBC initially benefit from preoperative
46 (neoadjuvant) chemotherapy (NAC); however, about 30%–50% develop resistance, leading to poor overall
47 survival rates[4,5]. Accumulating evidence indicates that cancer cells enter a reversible drug-tolerant
48 persister (DTP) cell-state to evade chemotherapy-induced cell death, leading to incomplete response
49 and/or recurrence[6–8]. DTP cells are characterized by a slow-cycling rate, stem-like traits (including the
50 expression of stem cell- and epithelial-to-mesenchymal (EMT) -markers), and a drug-resistant
51 phenotype[6–8]. One crucial distinction between DTP cells and cancer stem cells (CSCs) is that the DTP cell-
52 state is a rapidly acquired, dynamic, and reversible state – cycling between sensitive and resistant
53 phenotypes[8]. Remarkably, various chemotherapeutic agents, each with distinct mechanisms of action,
54 have demonstrated the ability to mediate the enrichment of DTP cells[9], suggesting the existence of
55 common cellular mechanisms driving drug resistance among diverse therapeutic approaches.

56 Drug tolerant cell-enrichment and drug resistance have conventionally been attributed to the selection of
57 pre-existing resistant (stem)-cell population(s) (referred to as intrinsic or Darwinian selection)[10]. However,
58 recent research using genomic and transcriptomic deep sequencing of matched longitudinal (pre- and
59 post-NAC treatment) TNBC patient and patient-derived xenograft (PDX) samples have also highlighted the
60 role of acquired (drug-induced) resistance during chemotherapy[11,12]. Here, cancer cells undergo profound
61 transcriptional changes in response to chemotherapeutic aggression, effectively acquiring new
62 transcriptional expression profiles that promote their survival and are believed to constitute a defensive
63 mechanism against treatment pressure. Notably, the enhanced phenotypic plasticity of TNBC enables a
64 rapid and early acquisition of a drug-tolerant state[13,14]. These findings collectively emphasize that therapy
65 is not only a selective force acting on pre-existing resistant cells, but also a driver of signaling cues that
66 lead to cellular transcriptional reprogramming, cell identity switching, and the emergence of DTP cell-
67 populations. Even though recent studies have focused on the genomic, epigenetic, and transcriptomic
68 contributions to TNBC tumor evolution and cell plasticity during treatment[11,15], knowledge concerning the
69 signaling pathways and mechanisms that operate during the early stages of drug tolerant cell(s)
70 emergence in response to chemotherapy remains limited.

71 The Wnt/β-catenin signaling pathway regulates a variety of cellular processes, including cell fate
72 commitment, differentiation, proliferation, and stem cell maintenance[16,17]. Wnt proteins (Wnts) are a
73 family of 19 secreted, glycosylated, and palmitoylated ligands which primarily interact with Frizzled (FZD)
74 receptors and/or low-density-lipoprotein receptor-related proteins 5/6 (LRP5/6) to promote activation of
75 the canonical (β-catenin-dependent) or non-canonical (β-catenin-independent) pathways[18]. Activation of
76 the canonical Wnt signaling pathway leads to stabilization of β-catenin promoting the transcription of
77 target genes. Wnt signaling is potentiated by the presence of R-spondin (RSPO) ligands, binding Leu-rich
78 repeat-containing G-protein coupled receptor 4-6 (LGR4-6) co-receptors preventing FZD receptor
79 degradation[18].
80 When dysregulated, Wnt signaling is a driver of tumorigenesis and chemoresistance in several human
81 cancers, including colorectal, liver, gastric cancer or TNBC. Importantly, activation of the canonical Wnt
82 signaling pathway and β-catenin stabilization have been correlated with unfavorable prognosis in patients
83 with TNBC[19–24]. Due to its capacity in regulating cell cycle, lineage commitment, and stem cell
84 maintenance, activation of the canonical Wnt signaling pathway is associated with a pro-proliferative and
85 cancer stem cell state[16,20,21,25]. Current research has predominantly focused on understanding the role of
86 Wnt signaling activation in TNBC tumors under baseline or unchallenged conditions, overlooking the
87 dynamics occurring during chemotherapeutic treatment[24,26,27].
88
89 Identifying and subsequently targeting the introductory, non-genetic events responsible for the
90 enrichment of drug-tolerant cell-populations in TNBC could pave the way for novel therapeutic strategies
91 to prevent treatment resistance. First, using TNBC cell lines, we show that *de novo* Wnt transcriptional
92 activation precedes drug-tolerant cell(s) enrichment regardless of the chemotherapeutic agent (docetaxel
93 or carboplatin) used. Activation of the Wnt signaling pathway by cytotoxic treatment was not limited *to in*
94 *vitro* 2D-cultured TNBC cell lines but was also consistently observed in 3D-cultured TNBC patient-derived
95 organoid (PDO) models as well as *in vivo* xenograft models. Furthermore, analysis of paired (NAC-treated,
96 pre- vs. post-treatment) BC patient datasets, of which patients did not achieve pathological complete
97 response (pCR), also showed differential enrichment of the Wnt signaling pathway. Following
98 transcriptomic and functional analyses of chemotherapy-treated Wnt^{High} cells, we observed a notable
99 correlation between Wnt-activation and the acquisition of DTP cell features. This association was
100 evidenced by a significant transcriptional correlation with an embryonic diapause gene signature, reduced
101 proliferation, and enhanced resistance capacity to chemotherapy. Further analysis revealed that

102 chemotherapy-induced Wnt-activation is mediated through increased expression and secretion of Wnt
103 ligands and/or Wnt enhancers.
104 We demonstrate that combinatorial, rather than sequential, treatment involving concomitant
105 pharmacological inhibition of Wnt ligand-secretion alongside chemotherapy hinders chemotherapy-
106 induced Wnt-activation and significantly sensitizes TNBC cell lines, xenograft models, and PDO models to
107 chemotherapy. Our findings suggest that patients undergoing chemotherapy treatment may potentially
108 encounter aberrant activation of the Wnt signaling pathway leading to drug-tolerant cell enrichment. This
109 implies that a combinatorial treatment strategy involving both Wnt ligand secretion-inhibition and
110 chemotherapy might effectively target the initial mechanisms involved in the enrichment and/or
111 acquisition of a DTP cell-phenotype while subsequently providing clinical benefits for patients with TNBC
112 undergoing systemic chemotherapy.
113

RESULTS

Wnt-transcriptional activation precedes drug-tolerant cell(s) enrichment upon chemotherapeutic treatment

To study the molecular basis of drug-tolerant cell(s) emergence or enrichment during therapy, we recapitulated this phenomenon *in vitro*. MDA-MB-231, MDA-MB-468, and PDC-BRC-101 TNBC cell lines were subjected to two separate chemotherapeutic agents: docetaxel (DOC) and carboplatin (CAR). These agents operate through different mechanisms of action, with DOC promoting microtubule stabilization and preventing depolymerization, and CAR inducing DNA damage[28,29]. IC50 concentrations (at 72h) were determined for each chemotherapeutic agent for every cell line and used in successive studies (Supplementary Fig. S1a-f). To assess changes in the frequency of putative drug-tolerant cells under chemotherapeutic pressure, the enzymatic activity of aldehyde dehydrogenase 1 (ALDH1), a functional stem cell marker in solid tumors whose expression is linked to drug resistance and the DTP cell-phenotype in TNBC[30,31], was assessed. Treatment of all TNBC cell lines with IC50 concentrations of either DOC or CAR led to a significant increase in the levels of $ALDH^+$ cells compared to untreated (UNT) conditions at 96hours(h) but not at 48h (Fig. 1a-c) indicating a time-dependent effect on drug-tolerant cell(s) enrichment following chemotherapeutic treatment.

To gain insights into the signaling cues preceding and, potentially, driving this chemotherapy-mediated enrichment of drug-tolerant ($ALDH^+$) cells at 96h, we performed bulk transcriptomic analysis of mRNA-sequenced samples obtained from viable/drug-tolerant ($DAPI^-$) MDA-MB-231 cells treated with either DOC or CAR at 72h (Supplementary Fig. S1g-i). Gene Set Enrichment Analysis[32] (GSEA) using MSigDB[33] datasets on differentially expressed genes (DEGs – Supplementary Fig. S1h, i, and Supplementary Table 1) between DOC vs. UNT or CAR vs. UNT (FC > 1.5, p-val ≤ 0.05) identified an array of Hallmarks significantly enriched in DOC or CAR treatments, including Apoptosis, p53 Pathway, and Interferon Gamma Response, which align with the expected cell stress induced by chemotherapeutic exposure (Fig. 1d, Supplementary Fig. S1j, k and Supplementary Table 2)[15]. Conversely, Hallmarks associated with cell cycle regulation were downregulated in DOC and CAR treatments (Fig. 1d) in line with findings of previous reports[15,34]. Interestingly, EMT and Hypoxia, both associated with tumorigenesis and drug-tolerance, were enriched in response to chemotherapeutic exposure (Fig. 1d and Supplementary Fig. S1j, k)[35,36].

To elucidate common transcriptomic alterations among distinct chemotherapeutic agents, we performed Gene Ontology (GO) analysis using the commonly (DOC & CAR vs. UNT) upregulated (1381) genes shared between both drugs (Fig. 1e). GO analysis repeatedly highlighted a significant enrichment of (positive)

146 regulation of Canonical Wnt signaling, which was corroborated with an enrichment in the expression of
147 Wnt-targets (*AXIN2* and *LGR5*) and upstream regulators and activators (*WLS* and *WNT2B*) of the pathway
148 (Fig. 1f, g). Conversely, GO analysis using commonly downregulated (785) genes shared between both
149 drugs highlighted significant enrichment in processes related to cell cycle regulation and progression
150 (Supplementary Fig. S1l, m).
151 Western Blot analysis of active (non-phosphorylated) β-catenin in TNBC cell lines confirmed increased
152 levels of active β-catenin, as early as 24 h post-treatment, and prolonged for up to 6 days (Fig. 1h-j).
153 Consequently, the expression levels of Wnt signaling target-genes (*AXIN2* and *LGR5*) showed a significant
154 increase, mirroring the elevated expression of stemness-associated markers (*SOX2*, *POU5F1*, and *NANOG*)
155 (Fig. 1k-m)[37–39].
156 Our data reveals an upregulation of canonical Wnt signaling activity preceding ALDH-enrichment. Notably,
157 this enrichment or activation of the Wnt signaling pathway appears to be a common phenomenon shared
158 among various TNBC cell lines and in response to two distinct cytotoxic treatments.
159

160 **Induction of transient *de novo* Wnt signaling transcriptional activation in response to**
161 **chemotherapy in TNBC cell lines**
162
163 To gain a more comprehensive understanding and an ability to monitor the kinetics orchestrating
164 chemotherapy-mediated Wnt signaling enrichment at the population level in living cells, we generated
165 clonal MDA-MB-231, MDA-MB-468, and PDC-BRC-101 TNBC cell lines carrying a stable integrated Wnt-
166 transcriptional (β-catenin-TCF/LEF-mediated transcriptional activity) reporter (TOP-GFP/TGP lines)[40] (Fig.
167 2a). We observed a range of TOP-GFP expression patterns in all three TNBC cell lines cultured in basal
168 conditions, with an approximate 6%, 2.5%, and 10% GFP^+ (referred to hereafter as Wnt^{High}) cells in MDA-
169 MB-231-TGP, MDA-MB-468-TGP, and PDC-BRC-101-TGP cell lines, respectively (Fig. 2a and Supplementary
170 Fig. S2a – top panel). Stimulating transcriptional activation levels of the Wnt signaling pathway with
171 CHIR99021, a small molecule serving as a GSK3β inhibitor, resulted in high levels of GFP-expression –
172 reaching >97% Wnt^{High} cells – confirming the fidelity of the reporter cell lines (Supplementary Fig. S2a –
173 bottom panel and S2b). Upon exposure to either DOC or CAR agents, we observed a significant increase in
174 the percentage of Wnt^{High} cells in viable/drug-tolerant ($DAPI^-$) cells compared to UNT (Fig. 2b-d and
175 Supplementary Fig. S2c). Prolonged exposure to either therapeutic agent for 6 days maintained or
176 increased the percentage of transcriptional Wnt^{High} cells (Fig. 2b-d), confirming that the enrichment and/or
177 induction of Wnt^{High} cells is one of the early events directing drug-tolerance. Intriguingly, we observed that
178 the median fluorescence intensity (MFI) of the GFP recorded in the chemotherapy-treated Wnt^{High}

179 population was significantly higher than that of the UNT Wnt^{High} population (Supplementary Fig. S2d),
180 suggesting that chemotherapy treatment not only augments the percentage of transcriptionally Wnt-
181 active cells in the drug-tolerant population but also enhances the levels of transcriptional Wnt-activation.
182 While live-cell imaging analysis of MDA-MB-231-TGP and PDC-BRC-101-TGP TNBC cell lines under UNT
183 conditions did not reveal significant changes in the levels of Wnt^{High} cells (Fig. 2e and Supplementary Fig.
184 S2e – black lines), treatment with either DOC or CAR resulted in a gradual enrichment of Wnt^{High} cells over
185 a similar chemo-culture timespan (Fig. 2e and Supplementary Fig. S2e), consistent with our previous FACS-
186 based results.
187 To visualize Wnt-transcriptional activation dynamics at single-cell resolution, we tracked the original Wnt-
188 state of Wnt^{High} cells (starting at 60h back to 0h) under UNT or chemotherapy-treated conditions. In UNT
189 conditions, 55% of Wnt^{High} cells in the MDA-MB-231-TGP cell line observed at 60h were initially Wnt^{High} at
190 T_0, while 34% were activated during the culture span (mode #2 and #1, respectively) (Fig. 2f, g,
191 Supplementary rep. images Fig. S2f – top panel, and Supplementary Videos SV1, 2). In contrast, under DOC
192 or CAR treatment conditions, the majority of Wnt^{High} cells at 60h (58% and 55%, respectively) were *de*
193 *novo*-activated during treatment, indicating chemotherapy-induced Wnt-activation in initially Wnt^{Low} cells
194 (GFP^{-} at T_0 – mode #1). Conversely, only 27% and 34% of Wnt^{High} cells in DOC and CAR treatment conditions
195 were initially Wnt^{High} at T_0 (mode #2) (Fig. 2h, i, rep. images Fig. 2j, k, Supplementary rep. images Fig. S2f –
196 middle and bottom panel, and Supplementary Videos SV3-6). These findings suggest that chemotherapy-
197 induced Wnt pathway-enrichment mainly results from *de novo* activation rather than only passive
198 selection of initially Wnt^{High} cells. Additional modes of Wnt-transcriptional activation dynamics were
199 observed in a minority of cases (mode #3 and #4) while cells that fell out of the imaging frame were
200 considered of unknown origin/state (mode #5). In accordance with these findings, similar observations
201 were validated using the PDC-BRC-101-TGP cell line (Supplementary Fig. S2g-i).
202 Next, we assessed the population dynamics of chemotherapy-induced Wnt^{High} cells after treatment was
203 halted (Fig. 2l). Interestingly, the percentage of Wnt^{High} cells was stabilized or even increased upon
204 chemotherapy removal for up to 3 weeks (Fig. 2m-p). Prolonged culture of these cells for 4 weeks in
205 chemo-free conditions resulted in a significant reduction in the percentage of Wnt^{High} cells, re-establishing
206 the Wnt-population to levels similar to that of UNT/basal-cultured cells. This data indicates that the
207 chemotherapy-induced Wnt^{High} phenotype is transient and reversible at the population level once
208 treatment pressure is removed (Fig. 2m-p and Supplementary Fig. S2j).
209 Altogether, these findings show that the Wnt^{High} phenotype results namely from a *de novo* chemotherapy-
210 driven action rather than solely representing a manifestation of an inherently chemotherapy-resistant

211 subpopulation selected under treatment pressure. Notably, upon chemotherapy removal, Wnt-activity
212 levels revert to baseline levels, indicating a transient Wnt^{High} state dependent on chemotherapy pressure.
213

214 **Bulk mRNA-sequencing of transcriptionally differential Wnt-populations reveals that**
215 **chemotherapy-treated Wnt^{High} cells display DTP cell-properties**
216
217 To unravel the transcriptional discrepancies between the Wnt^{Low} and Wnt^{High} populations, we conducted
218 bulk transcriptomic analysis on mRNA-sequenced samples derived from viable/drug-tolerant ($DAPI^{-}$) MDA-
219 MB-231-dTGP sorted populations in chemotherapy-treated conditions (Supplementary Fig. S3a)[41]. Gene
220 set variation analysis (GSVA) revealed a plethora of MSigDB Hallmark signatures from DEGs between CAR
221 or DOC (FC > 1.5, p-val ≤ 0.05) in Wnt^{High} vs. Wnt^{Low} sorted cells that were differentially up- or down-
222 regulated (Supplementary Fig. S3b, c, and Supplementary Tables 3-5).
223 As expected, the Wnt signaling pathway was significantly and positively associated in CAR- and DOC-sorted
224 Wnt^{High} populations compared to Wnt^{Low} populations (Fig. 3a and Supplementary Fig. S3e). While a few
225 signatures exhibited drug-dependent associations, most differentially regulated hallmarks followed a
226 similar associative trend among sorted chemo-treated Wnt^{High} and Wnt^{Low} cells observed across both drug
227 treatments (Fig. 2a-d and Supplementary Fig. S3e). Notably, developmental signaling pathways, including
228 Hedgehog, Notch, IL-6/JAK/STAT3, and TGF-β signaling, along with hallmarks linked to tumor progression,
229 stemness capacity, and metastasis[42–44] (e.g., Angiogenesis and EMT), displayed a significant positive
230 association with Wnt^{High} populations in comparison to Wnt^{Low} populations (Fig. 3a, b, and Supplementary
231 Fig. S3e). Conversely, the TNF-α signaling pathway via the NF-κB pathway notably exhibited a significant
232 negative association with Wnt^{High} cells (Fig. 3a and Supplementary Fig. S3e) aligning with previous findings
233 suggesting that active β-catenin can attenuate transcriptional NF-κB activity in breast cancer[45].
234 Even though Wnt pathway-activation has been shown to correlate with increased proliferation[46], our
235 transcriptional analysis revealed that Wnt^{High} cells negatively correlated with transcriptional signatures of
236 proliferation, as evidence by significant reduction of a MYC target, G2M checkpoint, and E2F target
237 signatures across chemo-treated Wnt^{High} samples (Fig. 3c and Supplementary Fig. 3e)[19,46]. In addition, a
238 significant negative association was also identified for chemo-treated Wnt^{High} cells and
239 Caspase3/Apoptosis signatures (Fig. 3d and Supplementary Fig. 3e). Notably, the coordinated upregulation
240 of hallmarks associated with Notch and EMT alongside downregulation of MYC targets and
241 Caspase3/Apoptosis signatures observed in Wnt^{High} cells mirrors crucial cellular processes involved in the
242 functionality of DTPs[9,47] suggesting that Wnt^{High} cells may transcriptionally resemble DTP cells (Fig. 3e).

243 A remarkable recent finding has been the observation that cancer DTP cells and embryonic diapause cells
244 share an extensive transcriptional profile[9,47,48]. Recently, Rehman et al. identified a distinctive embryonic
245 diapause gene signature which significantly correlated with cancer DTP cells. Interestingly, we observed a
246 significant positive association between the diapause/DTP gene signature and sorted chemo-treated
247 Wnt^{High} cells, further providing evidence regarding Wnt^{High} cells resembling a transcriptional DTP cell-state
248 (Fig. 3f).
249 We aimed to explore if the observed transcriptional changes in Wnt^{High} cells under chemotherapy pressure
250 were already pre-existing in UNT conditions. Despite a positive correlation between Wnt^{High} cells obtained
251 from UNT conditions and the Wnt/β-catenin hallmark signature, the association was not statistically
252 significant (Fig. 3a), consistent with our previous data highlighting lower levels of Wnt signaling-
253 activity/intensity in UNT samples (Supplementary Fig. S2d). Interestingly, UNT-derived Wnt^{High} cells
254 exhibited overall positive associations with developmental signaling pathways and significant positive
255 associations with EMT, while exhibiting significant negative associations with cell cycle hallmarks, including
256 MYC targets (Fig. 3a-d and Supplementary Fig. S3e). Moreover, unchallenged Wnt^{High} cells displayed a
257 notable correlation with the diapause/DTP gene signature (Fig. 3e, f), highlighting transcriptional Wnt-
258 activity as a functional marker for early DTP cells. The significance of this correlation becomes more
259 apparent in chemo-treated conditions, where transcriptional Wnt-activation is strongly exacerbated.
260 Functional analyses confirmed reduced cell proliferation measured by cell number (Fig. 3g) observed in
261 chemo-sorted Wnt^{High} compared to Wnt^{Low} populations (Fig. 3h). Furthermore, co-staining of GFP-
262 expression (reporter for Wnt-activity) alongside the apoptotic marker Annexin V revealed that Wnt^{High} cells
263 displayed reduced apoptotic activity confirming their enhanced drug-tolerant state (Fig. 3i).
264 In summary, our comprehensive data reveals that chemotherapy-treated Wnt^{High} cells share a
265 transcriptional profile with cancer DTP cells including a recently identified diapause/DTP gene signature.
266 Functional assessments further confirm a drug-tolerant state strongly pronounced in chemotherapy-
267 enriched Wnt^{High} cells suggesting that transcriptional Wnt-activity might serve as a functional indicator of
268 early drug-tolerance, especially following chemotherapeutic challenge.
269

270 **Chemotherapeutic treatment induces elevated transcriptional expression of Wnt ligands, Wnt**
271 **enhancers, and Wnt secretion machinery components**
272

273 The Wnt signaling pathway is highly conserved and activated via the binding of (19) extracellular Wnt
274 ligands (Wnts) to membrane receptors[19]. Secretion of Wnt ligands requires the action of the

275 acyltransferase Porcupine (PORCN) followed by Wntless/evenness interrupted (WLS/Evi) which supports
276 transport of Wnts from the Trans-Golgi Network to the plasma membrane. In addition, the Rspo protein
277 family has been shown to enhance Wnt ligand activity to further promote Wnt pathway-activation[18,19].
278 RT-qPCR screening, focusing on established canonical Wnt ligands (Wnt-1, Wnt-2, Wnt-2b, Wnt-3, Wnt-3a,
279 and Wnt-7b), Wnt ligand enhancers/amplifiers (Rspo1-4), and Wnt secretion machinery components
280 (WLS/Evi and PORCN), revealed that the transcriptional expression of key genes, including *WNT2B*, *WNT3*,
281 *WNT3A*, *WNT7B*, *RSPO1*, *RSPO3*, *WLS*, and *PORCN* was found to be steadily expressed in basal conditions
282 across all analyzed TNBC cell lines (Supplementary Fig. S4a-c).
283 Importantly, these genes exhibited a consistent and statistically significant increase in expression levels
284 under chemotherapy-treatment conditions (Fig. 4a-c) suggesting that chemotherapeutic exposure actively
285 promotes elevated transcription levels of several key components involved in canonical Wnt pathway-
286 activation.
287 Subsequently, following chemotherapy removal and under one week chemo-recovery conditions, the
288 majority of Wnt-activation components maintained elevated expression levels (Fig. 4d, e – pink bars)
289 However, after four weeks of culture in chemo-free conditions and coinciding with the previous results
290 displaying the return of Wnt^{High} cells to basal levels (Fig. 2m-p), we observed a corresponding decrease in
291 expression level patterns of Wnt-activation components (Fig. 4d, e – light blue bars). This correlation
292 between the expression levels of Wnt-activation components and the dynamic induction of a Wnt^{High}
293 population highlights the transient nature of chemotherapy-induced Wnt-activation (Fig. 2m-p), providing
294 a possible mechanism for the enrichment of a Wnt^{High} population in response to treatment.
295 Western blot analysis confirmed the upregulation of the Wnt ligand Wnt-2b and the acyltransferase
296 PORCN, in response to either DOC or CAR treatments across all analyzed TNBC cell lines (Fig. 4f-k).
297 Treatment of chemo-naïve cells with concentrated conditioned media (CM) derived from MDA-MB-231
298 and MDA-MB-468 TNBC cell lines (Fig. 4l) confirmed increased and functional presence of Wnt ligands in
299 media collected under one week chemo-recovery conditions, resulting in a significant increase in Wnt^{High}
300 cells when compared to chemo-naïve cells treated with UNT CM (Fig. 4m, n). In a parallel experiment, we
301 co-cultured chemo-naïve (MDA-MB-231-mCherry-TGP) cells with chemo-recovering (MDA-MB-231) cells
302 (Fig. 4o). This co-culturing approach similarly resulted in a substantial and statistically significant increase
303 in the percentage of Wnt^{High} cells within the chemo-naïve cell population (Fig. 4p).
304 In summary, our findings demonstrate that chemotherapeutic treatment leads to elevated expression
305 levels of Wnt ligands, -enhancers, and -components of the Wnt secretory apparatus. Significantly,

306 concentrated CM obtained from chemo-treated and recovered cells induces an enrichment in the Wnt^{High}
307 cell population, substantiating the functional impact of the chemo-secreted factors.
308

309 **Concomitant inhibition of Wnt ligand secretion enhances chemotherapeutic sensitivity in TNBC**
310 **cell lines**
311
312 We stably transduced MDA-MB-231, MBD-MB-468, and PDC-BRC-101 TNBC cell lines with lentiviral shRNA
313 constructs designed to silence the acetyltransferase PORCN, avoiding the O-palmitoylation and functional
314 secretion of Wnt ligands[49,50]. The silencing of PORCN led to a substantial reduction (approx. 80-90%) in
315 PORCN mRNA levels (Supplementary Fig. S5a-c). PORCN silenced (shPORCN#1) cell lines exposed to either
316 chemotherapeutic agent revealed reduced levels of active β-catenin or percentage of Wnt^{High} cells
317 compared to control (shPLKO) lines, confirming an essential role for PORCN in chemotherapy-induced Wnt-
318 activation (Fig. 5a-c and Supplementary Fig. S5d). While the silencing of PORCN had no impact on cell
319 viability in basal (UNT) culture conditions, we observed a marked and significant increase in levels of
320 apoptotic (Annexin V^{+} and DAPI^{+}) cells in shPORCN#1 TNBC cell lines compared to shPLKO lines, indicating
321 a strong sensitization role of PORCN-inhibition (Fig. 5d-f). We validated the reduction of the
322 chemotherapy-induced Wnt^{High} population and increased sensitization to chemotherapy using a second
323 independent lentiviral shRNA construct targeting PORCN (Supplementary Fig. S5e-g) confirming that
324 genetic inhibition of Wnt ligand secretion effectively hinders the advent of a chemotherapy-induced
325 Wnt^{High} population while significantly enhancing the sensitization of TNBC cell lines to chemotherapy.
326 In recent years, several pharmacological inhibitors of the acyltransferase PORCN, which effectively abolish
327 the secretion of Wnt ligands, have been developed. These PORCN inhibitors have demonstrated their
328 efficacy in inhibiting Wnt signaling in various solid tumors, including Wnt-deregulated colon cancer and
329 various TNBC cell lines or murine models in baseline conditions[51,52]. Given our previous findings that the
330 Wnt signaling pathway is activated in response to chemotherapeutic treatment, we sought to investigate
331 whether pharmacological inhibition of PORCN could also prove effective in curbing Wnt-activation induced
332 under treatment pressure. We conducted two distinct experimental setups to further investigate this
333 matter. In the first setup, we pre-treated MDA-MB-231, MBD-MB-468, and PDC-BRC-101 TNBC cell lines
334 with the Inhibitor of Wnt Production (IWP-2) for 48h followed by the application of either DOC or CAR
335 agents (Sequential Treatment)[53]. In the second setup, we applied chemotherapeutic treatment
336 simultaneously and in combination with IWP-2 (Combinatorial Treatment).
337 Pre-treatment (sequential treatment strategy – Fig. 5g) of MDA-MB-231, MBD-MB-468, and PDC-BRC-101
338 TNBC cell lines with IWP-2 for 48h led to a notable and significant reduction in the percentage of Wnt^{High}

339 cells as well as a reduction in stem cell marker expression (Fig. 5h, j) with no effects on cell viability
340 (Supplementary Fig. S5h). However, upon chemotherapy addition, we observed robust chemotherapy-
341 induced Wnt-activation and increased stem cell marker expression in IWP-2 pre-treatment conditions
342 when compared to sole chemo-treatment in all TNBC cell lines (Fig. 5i, j). Notably, pre-treatment with IWP-
343 2 followed by chemotherapy addition did not result in increased cell death nor sensitization to either agent
344 (Supplementary Fig. S5i-k), suggesting that a strategy to target *a priori* existent Wnt^{High} population might
345 not be sufficient to prevent chemotherapy-induced Wnt-activation and its subsequent implications.
346 In the second setup (combinatorial treatment strategy – Fig. 5k), simultaneous treatment of TNBC cell lines
347 with either DOC or CAR therapeutic agent in combination with IWP-2 led to a significant decrease in the
348 percentage of Wnt^{High} cells (Fig. 5l) and a strong reduction in stem cell marker expression (Fig. 5m). This
349 underscores the critical role of Wnt ligand secretion in this acquired Wnt-activation phenomenon.
350 Intriguingly, combinatorial treatment involving chemotherapeutic agents alongside IWP-2 resulted in a
351 substantial increase in apoptotic cell death across all analyzed TNBC cell lines compared to treatment with
352 either chemotherapeutic agent alone (Fig. 5n). Interestingly, we observed that the supplementation of
353 IWP-2 alongside chemotherapy resulted in significant downregulation of drug-tolerant associated genes,
354 *SURVIVIN* and *ABCB1* (Supplementary Fig. S5l)[54,55]. Furthermore, using a second pharmacological PORCN
355 inhibitor, WNT-974 (LGK-974, currently tested in phase I/II clinical trials)[56,57] resulted in similar results
356 obtained with Wnt ligand secretion-inhibitor IWP-2 (Supplementary Fig. 5m-r).
357 In summary, our findings collectively demonstrate the essential role of Wnt ligand secretion in driving
358 chemotherapy-induced Wnt-activation and chemoresistance. Notably, simultaneous, rather than
359 sequential, treatment with chemotherapeutic agents and pharmacological Wnt ligand secretion-inhibition
360 can significantly curb chemotherapy-induced Wnt-activation and ultimately sensitize TNBC cell lines to
361 chemotherapy.
362
363
364 **Inhibition of Wnt ligand secretion and chemotherapeutic treatment synergistically sensitize *in***
365 ***vivo* xenograft TNBC model to treatment**
366
367 A precise and complete understanding of Wnt-activation kinetics and dynamics in response to
368 chemotherapeutic treatment in *in vivo* models is lacking. To shed some light on this phenomenon, we
369 engineered the TNBC cell line MDA-MB-231 with the Wnt-transcriptional reporter TOPFLASH, a β-catenin-
370 responsive firefly luciferase reporter plasmid compatible for use with the *in vivo* live imaging system (IVIS)
371 (Fig. 6a)[40].

372 Treatment with either DOC or CAR[58,59] resulted in a significant overall decrease in tumor volume when
373 compared to the vehicle (VEH) treated group (Fig. 6b, c). Notably, at the administered doses, no significant
374 changes in mouse body weight were observed during the three weeks of treatment (Supplementary Fig.
375 S6a). We observed, as early as 48h and 72h (for DOC and CAR, respectively) upon chemotherapeutic
376 administration, a significant upregulation in transcriptional Wnt-activation recorded by IVIS (Fig. 6d, e and
377 representative image Supplementary Fig. S6b). Notably, this activation started to decrease as the week
378 progressed following the 1st dose-administration and again increased significantly 48h and 72h (for DOC
379 and CAR, respectively) following administration of the 2nd and 3rd dose (Fig. 6d, e) highlighting the dynamic
380 behavior of chemotherapy-induced Wnt-activation *in vivo*. Gene expression analysis on the resected
381 tumors following the 3rd and final cycle of chemotherapeutic administration revealed elevated expression
382 of Wnt-targets (*AXIN2* and *LEF1*), stemness markers (*POU5F1* and *SOX2*), Wnt ligands and -enhancers
383 (*WNT2B*, *WNT3A*, *WNT7B*, *RSPO1*, and *RSPO3*), and Wnt secretion machinery components (*WLS* and
384 *PORCN*) (Fig. 6f and Supplementary Fig. S6c, d) in chemotherapy-treated groups.
385 We next proceeded to assess whether a combinatorial treatment strategy encompassing the use of
386 chemotherapy with a pharmacological Wnt ligand secretion-inhibitor (Fig. 6g) could abrogate Wnt-
387 activation and lead to tumor sensitization, as indicated in our previous *in vitro* findings. Administration of
388 LGK-974 alone had no discernible effect on tumor growth (Fig. 6h, i, and Supplementary Fig. S6e)[60,61].
389 Conversely, the combination of LGK-974 with either DOC or CAR treatment resulted in a substantial and
390 significant decrease in Wnt pathway-activation, correlating with a marked reduction in tumor volume
391 compared to solo chemo-treated or VEH-groups (Fig. 6h-k and Supplementary Fig. S6e). Notably, LGK-
392 treatment, sole or in combination with either chemotherapeutic agent, had no significant effect on mouse
393 body weight observed during the three weeks of treatment (Supplementary Fig. S6f).
394 Response Evaluation Criteria in Solid Tumors (RECIST) analysis was performed to assess tumor response to
395 treatment, categorizing objective outcomes into progressive disease (PD), stable disease (SD), partial
396 response (PR), and complete response (CR). In the VEH-group, 75% (6/8) of tumors were classified as PD,
397 and 25% (2/8) were classified as SD (Fig. 6l). Sole LGK-974 treatment showed no difference in RECIST
398 classifications (75% PD and 25% SD) compared to VEH-conditions, indicating minimal impact on tumor
399 burden (Fig. 6l). In solo DOC- or CAR-treated groups, RECIST analysis classified 100% of tumors as SD,
400 demonstrating the efficacy of DOC or CAR treatments in controlling tumor growth (Fig. 6l). In the DOC+LGK
401 treatment arm, LGK-974 supplementation significantly improved objective response with tumors classified
402 as 28.6% SD (2/7) and 71.4% PR (5/7) (Fig. 6l), compared to sole DOC-treatment (100% SD). Similarly, in

403 the CAR+LGK treatment arm, tumors were classified as 42.8% SD (3/7), 28.6% PR (2/7), and 28.6% CR (2/7),
404 highlighting the positive impact of combining chemotherapy with Wnt secretion-inhibition (Fig. 6l).
405
406 Our study comprehensively characterizes the dynamics of the Wnt signaling pathway in chemotherapy-
407 treated tumors within an *in vivo* setting. Furthermore, we demonstrate that a treatment regimen
408 combining chemotherapy and Wnt ligand secretion-inhibition significantly diminishes the enrichment of
409 Wnt pathway-activation and curbs tumor growth.
410

411 **Preclinical PDO models recapitulate chemotherapy-mediated Wnt-activation and sensitization**
412 **to synergistic Wnt ligand secretion inhibition**
413
414 To investigate whether Wnt/β-catenin signaling is enriched in breast cancer patients following exposure to
415 chemotherapy, we conducted transcriptomic analysis on two patient-derived DNA microarray datasets
416 containing paired (pre- and post-NAC treated) samples that did not achieve pCR (GSE87455 and GSE21974
417 – Supplementary Fig. S7a, b)[62–64](Supplementary Tables 6, 7). Hallmarks and KEGG gene sets from the
418 human MSigDB database consistently identified the Wnt signaling pathway as significantly enriched in
419 tumor samples obtained from patients post-NAC treatment (Supplementary Fig. S7c-f) in both datasets.
420 We next investigated the effect of chemotherapeutic treatment and Wnt ligand secretion-inhibition on
421 pre-clinical 3D Patient Derived Organoid (PDO) models[65,66]. Two different PDO models, R1-IDC113 (113
422 BCO) and R2-IDC159A (159A BCO) (Fig. 7a and Supplementary Fig. S7g) were used. Typically, organoid
423 models are cultured in growth factor-dense medium[67], including Wnt ligand (Wnt-3a) and Wnt ligand-
424 enhancer (R-spondin3), possibly influencing studies of Wnt signaling pathway dynamics. Culturing of
425 either cancer organoid model for four passages in a $Wnt^-/Rspo^-$ breast cancer organoid (BCO) medium,
426 had no effects on the morphology, proliferation rate, or viability of either PDO model when compared to
427 a baseline ($Wnt^+/Rspo^+$) BCO medium (Supplementary Fig. S7h, i).
428 Upon exposure to IC50 concentrations of either DOC or CAR agents in a $Wnt^-/Rspo^-$ BCO media
429 (Supplementary Fig. S7j-m), both PDO models exhibited a substantial and statistically significant increase
430 in the expression levels of Wnt-target genes and stem cell markers, compared to UNT conditions (Fig. 7b,
431 c). Immunofluorescence analysis of active β-catenin levels confirmed increased Wnt-activation in both
432 PDO models following exposure to either chemotherapeutic agent (Fig. 7d and Supplementary Fig. S7n).
433 Additionally, our data confirmed significant elevation in the expression levels of Wnt ligands, -enhancers,
434 and -secretion machinery components in chemotherapy-treated PDO models when compared to UNT

435 conditions (Fig. 7e, f). Collectively, these results support the notion of robust Wnt signaling pathway-
436 activation in response to chemotherapeutic treatment in two distinct TNBC pre-clinical PDO models.
437 To investigate the efficacy of the combinatorial treatment strategy, both PDO models were exposed to Wnt
438 ligand secretion-inhibition alone and in combination with escalating concentrations of either
439 chemotherapeutic agent for 96h. Treatment of both PDO models with IWP-2 alone for 96h did not have
440 any effect on cell viability or proliferation (Supplementary Fig. S7o). However, the exposure of both PDO
441 models to chemotherapy in conjunction with IWP-2 demonstrated a significant reduction in the
442 percentage of viable cells compared to chemotherapeutic treatment alone (Fig. 7g-j). Interestingly, this
443 sensitization effect was most effective when IWP-2 was supplemented with sublethal concentrations of
444 chemotherapy (<16nM DOC and <50µM CAR, 113 BCO | <8nM DOC and <125µM CAR, 159A BCO).
445 In summary, our study demonstrates chemotherapy-induced Wnt-activation in TNBC pre-clinical models
446 and in post-NAC patient derived transcriptomic datasets. Notably, TNBC PDO models exhibited a robust
447 and enhanced sensitization to the combinatorial treatment comprising Wnt ligand secretion-inhibition
448 alongside sub-lethal chemotherapy (<determined IC50) concentrations. This finding underscores the
449 potential clinical significance of this combinatorial approach for breast cancer treatment.
450

DISCUSSION

The emergence of DTP cells during cancer treatment has become a focal point of oncological research, due to their pivotal role in drug resistance and tumor relapse. Our study delves into an early mechanism, delineating processes of therapy-driven evolution in cancer cells and the enrichment of drug-tolerant cells in response to treatment pressure in TNBC. Our findings reveal a significant enrichment in the percentage of a Wnt^{High} population alongside an increase in the intensity of Wnt-activation in various TNBC models subjected to distinct chemotherapeutic agents. Activation of the Wnt/β-catenin signaling pathway has been linked with CSC renewal and maintenance[19–21,25]. However, in contrast, we establish a significant transcriptional association between the Wnt^{High} population and DTP cells, including a unique diapause/DTP gene signature and a reduction of MYC targets hallmark; both recently correlated with cancer DTP cells[9,47]. Functional analyses confirmed that Wnt^{High} cells exhibit DTP cell-traits such as reduced proliferation and an enhanced capacity for drug tolerance[7,8] Furthermore, the dynamic, transient, and reversible behavior places chemotherapy-treated Wnt^{High} cells closer to the DTP cell criteria and apart from criteria of CSCs, providing a novel perspective for the poor clinical outcomes in TNBC patients with Wnt-deregulation[20,24,26]. This suggests that the transcriptional activation of the Wnt signaling pathway could serve as a distinctive marker for the early emergence of the DTP cell-phenotype, particularly in response to chemotherapeutic exposure.

Current clinical trials investigating PORCN inhibition in TNBC involve the use of a Wnt ligand-inhibitor as monotherapy or in combination with PDR001 (an anti-PD1 antibody), restricted to Wnt-deregulated cancers and excluding consideration of chemotherapy (NCT03447470 and NCT01351103)[56,57]. Our results suggest that combinatorial treatment involving Wnt ligand secretion-inhibition supplemented alongside chemotherapy sensitizes tumors to treatment and holds significant promise for future clinical trials in TNBC. Our study also underscores the importance of temporal considerations in treatment regimens. Crucially, we show that pre-treatment with PORCN inhibitors does not prevent a substantial increase in Wnt^{High} cells or stem cell marker expression once chemo-treatment is applied, indicating that patients undergoing chemotherapy might not benefit from initial treatment with Wnt-inhibitors. Therefore, our findings suggest that simultaneous treatment, rather than sequential treatment, with Wnt-inhibitors and chemotherapy might provide a solution to effectively control chemotherapy-induced drug tolerant cell-enrichment while simultaneously sensitizing tumors to the effects of chemotherapy.

Live-cell imaging, allowing the possibility to track and trace Wnt-reporter TNBC cell lines, revealed that, in contrast to unchallenged (UNT) culture conditions, chemotherapy-mediated enrichment of Wnt^{High} cells is

482 primarily observed in cells initially in a Wnt^{Low} state, indicating *de novo* activation of the pathway in
483 response to chemotherapeutic treatment. Furthermore, we noted a significant percentage of Wnt^{High} cells
484 in chemo-treated conditions that were initially in a transcriptionally Wnt-active state, suggesting that
485 intrinsic and acquired resistance mechanisms driven by Wnt-transcriptional activity are not mutually
486 exclusive and likely occur simultaneously.

487 The molecular mechanisms triggering the initial increased expression of Wnt ligands and Wnt enhancers
488 described in this article, or the transcriptional reprogramming previously described in other works in
489 chemotherapy-treated conditions, remain largely unknown[11,12]. Studies in other contexts, such as ovarian
490 cancer, have suggested that chemotherapy-induced stress may induce significant epigenetic changes,
491 indicating a potential role of epigenetic regulation in chemotherapy-induced Wnt pathway-activation[68,69].
492 Recent research shows that depletion of H3K27me3 (trimethylation of histone H3 at lysine 27) promotes
493 a drug-tolerant state in TNBC and highlights epigenetic regulation as an early event involved in promoting
494 chemoresistance[15]. In our RNA-seq analysis of MDA-MD-231 cells treated with DOC or CAR, we observed
495 around 2,500 upregulated expressed genes (DEGs) 72h post-treatment. Notably, more than 50% (1,650)
496 of these DEGs were common between DOC and CAR treatments, suggesting that the onset of
497 transcriptional reprogramming observed following treatment may be orchestrated by shared molecular
498 mechanisms, even when distinct drugs are used. One possibility is that cells exposed to stress posed by
499 chemotherapeutic pressure may activate pro-survival mechanisms and signaling cues. Interestingly, in
500 regenerative models like *Hydra*, an increase in Wnt ligand expression has been observed in cells
501 undergoing apoptosis as a regenerative pro-survival response to tissue damage[70]. In this article, we
502 propose a mechanistic model for acquired chemoresistance mediated via drug-tolerant cell(s) enrichment
503 in TNBC, comprising two distinct phases. Initially, cells sense environmental changes induced by
504 chemotherapeutic pressure, resulting in increased levels of Wnt ligand(s) and Wnt enhancer(s) transcripts,
505 accompanied by heightened Wnt ligand secretion. Subsequently, to adapt to these environmental
506 pressures, cells transcriptionally activate the Wnt signaling pathway, ultimately giving rise to a defensive
507 and chemotherapy-resistant Wnt^{High} phenotype.
508

509 In a recent study by Wang et al., a cell-autonomous mechanism was unveiled, shedding light on how
510 genotoxic treatment in breast cancer cells can activate the Wnt/β-catenin signaling pathway[71]. This
511 activation was mediated through OTULIN, a linear linkage-specific deubiquitinase, which exerted its
512 stabilizing influence on β-catenin through non-Wnt ligand-specific mechanisms. Notably, the OTULIN-
513 dependent stabilization of β-catenin, as detailed in Wang et al.'s work, manifested primarily during the

514 initial phases of drug treatment, with effects discernible for a maximum of 24h post-chemotherapy
515 exposure. Our current study, in contrast, introduces a novel perspective on chemotherapy-induced Wnt
516 pathway-activation, elucidating a mechanism reliant on Wnt ligands in diverse human TNBC cellular
517 models. Furthermore, our research reveals a sustained and prolonged incidence of chemotherapy-induced
518 Wnt pathway activation that extends well beyond the initial 24h window following treatment initiation.
519 We complement these observations with a comprehensive transcriptional and functional characterization
520 of the Wnt^{High} and Wnt^{Low} populations that emerge as a consequence of chemotherapeutic treatment.
521 Collectively, our findings underscore a previously unrecognized mechanism governing chemotherapy-
522 induced Wnt pathway-activation, emphasizing the vital role of Wnt ligands in this process. To further
523 expand our understanding, future investigations should explore whether ionizing radiation, similar to
524 chemotherapy, can also induce Wnt pathway-activation and whether this occurs via Wnt ligand-dependent
525 or independent mechanisms.
526 In summary, our research suggests that the secretion of Wnt ligands could play a pivotal role as an early
527 event enhancing the enrichment of DTP cell populations in TNBC and contribute to the development of
528 therapeutic resistance, particularly in response to chemotherapy. Therefore, a potential strategy to
529 address this challenge could involve targeting Wnt ligand-secretion successively hindering chemotherapy-
530 induced Wnt/β-Catenin pathway activation and subsequently diminishing the sustenance and enrichment
531 of DTP cell populations (Fig. 7k).
532

533 **REFERENCES**

534 1. Bianchini, G., De Angelis, C., Licata, L. & Gianni, L. Treatment landscape of triple-negative breast
535 cancer — expanded options, evolving needs. *Nat. Rev. Clin. Oncol.* **19**, 91–113 (2022).
536 2. Waks, A. G. & Winer, E. P. Breast Cancer Treatment. *JAMA* **321**, 288 (2019).
537 3. Nolan, E., Lindeman, G. J. & Visvader, J. E. Deciphering breast cancer: from biology to the clinic.
538 *Cell* **186**, 1708–1728 (2023).
539 4. Foulkes, W. D., Smith, I. E. & Reis-Filho, J. S. Triple-Negative Breast Cancer. *N. Engl. J. Med.* **363**,
540 1938–1948 (2010).
541 5. Liedtke, C. *et al.* Response to Neoadjuvant Therapy and Long-Term Survival in Patients With
542 Triple-Negative Breast Cancer. *J. Clin. Oncol.* **26**, 1275–1281 (2008).
543 6. Shi, Z.-D. *et al.* Tumor cell plasticity in targeted therapy-induced resistance: mechanisms and new
544 strategies. *Signal Transduct. Target. Ther.* **8**, 113 (2023).
545 7. Pu, Y. *et al.* Drug-tolerant persister cells in cancer: the cutting edges and future directions. *Nat.*
546 *Rev. Clin. Oncol.* **20**, 799–813 (2023).
547 8. Zhang, Z., Tan, Y., Huang, C. & Wei, X. Redox signaling in drug-tolerant persister cells as an
548 emerging therapeutic target. *eBioMedicine* **89**, 104483 (2023).
549 9. Rehman, S. K. *et al.* Colorectal Cancer Cells Enter a Diapause-like DTP State to Survive
550 Chemotherapy. *Cell* **184**, 226-242.e21 (2021).
551 10. Marusyk, A., Janiszewska, M. & Polyak, K. Intratumor Heterogeneity: The Rosetta Stone of
552 Therapy Resistance. *Cancer Cell* **37**, 471–484 (2020).
553 11. Kim, C. *et al.* Chemoresistance Evolution in Triple-Negative Breast Cancer Delineated by Single-
554 Cell Sequencing. *Cell* **173**, 879-893.e13 (2018).
555 12. Echeverria, G. V. *et al.* Resistance to neoadjuvant chemotherapy in triple-negative breast cancer
556 mediated by a reversible drug-tolerant state. *Sci. Transl. Med.* **11**, (2019).
557 13. Zawistowski, J. S. *et al.* Enhancer Remodeling during Adaptive Bypass to MEK Inhibition Is
558 Attenuated by Pharmacologic Targeting of the P-TEFb Complex. *Cancer Discov.* **7**, 302–321
559 (2017).
560 14. Risom, T. *et al.* Differentiation-state plasticity is a targetable resistance mechanism in basal-like
561 breast cancer. *Nat. Commun.* **9**, 3815 (2018).
562 15. Marsolier, J. *et al.* H3K27me3 conditions chemotolerance in triple-negative breast cancer. *Nat.*
563 *Genet.* **54**, 459–468 (2022).
564 16. Liu, J. *et al.* Wnt/β-catenin signalling: function, biological mechanisms, and therapeutic
565 opportunities. *Signal Transduct. Target. Ther.* **7**, 3 (2022).
566 17. Yang, K. *et al.* The evolving roles of canonical WNT signaling in stem cells and tumorigenesis:
567 implications in targeted cancer therapies. *Lab. Investig.* **96**, 116–136 (2016).
568 18. Niehrs, C. The complex world of WNT receptor signalling. *Nat. Rev. Mol. Cell Biol.* **13**, 767–779
569 (2012).
570 19. Xu, X., Zhang, M., Xu, F. & Jiang, S. Wnt signaling in breast cancer: biological mechanisms,
571 challenges and opportunities. *Mol. Cancer* **19**, 165 (2020).
572 20. Pohl, S.-G. *et al.* Wnt signaling in triple-negative breast cancer. *Oncogenesis* **6**, e310–e310 (2017).
573 21. Abreu de Oliveira, W. A., El Laithy, Y., Bruna, A., Annibali, D. & Lluis, F. Wnt Signaling in the
574 Breast: From Development to Disease. *Front. Cell Dev. Biol.* **10**, (2022).
575 22. Geyer, F. C. *et al.* β-Catenin pathway activation in breast cancer is associated with triple-negative
576 phenotype but not with CTNNB1 mutation. *Mod. Pathol.* **24**, 209–231 (2011).
577 23. Zhan, T., Rindtorff, N. & Boutros, M. Wnt signaling in cancer. *Oncogene* **36**, 1461–1473 (2017).
578 24. Khramtsov, A. I. *et al.* Wnt/β-Catenin Pathway Activation Is Enriched in Basal-Like Breast Cancers
579 and Predicts Poor Outcome. *Am. J. Pathol.* **176**, 2911–2920 (2010).

580 25. Zheng, H. *et al.* Targeted activation of ferroptosis in colorectal cancer via LGR4 targeting
581 overcomes acquired drug resistance. *Nat. Cancer* (2024) doi:10.1038/s43018-023-00715-8.
582 26. Geyer, F. C. *et al.* β-Catenin pathway activation in breast cancer is associated with triple-negative
583 phenotype but not with CTNNB1 mutation. *Mod. Pathol.* **24**, 209–231 (2011).
584 27. Dey, N. *et al.* Wnt signaling in triple negative breast cancer is associated with metastasis. *BMC*
585 *Cancer* **13**, 537 (2013).
586 28. Rottenberg, S., Disler, C. & Perego, P. The rediscovery of platinum-based cancer therapy. *Nat.*
587 *Rev. Cancer* **21**, 37–50 (2021).
588 29. Verweij, J., Clavel, M. & Chevalier, B. Paclitaxel (TaxolTM) and docetaxel (TaxotereTM): Not
589 simply two of a kind. *Ann. Oncol.* **5**, 495–505 (1994).
590 30. Dhanyamraju, P. K., Schell, T. D., Amin, S. & Robertson, G. P. Drug-Tolerant Persister Cells in
591 Cancer Therapy Resistance. *Cancer Res.* **82**, 2503–2514 (2022).
592 31. Raha, D. *et al.* The Cancer Stem Cell Marker Aldehyde Dehydrogenase Is Required to Maintain a
593 Drug-Tolerant Tumor Cell Subpopulation. *Cancer Res.* **74**, 3579–3590 (2014).
594 32. Subramanian, A. *et al.* Gene set enrichment analysis: A knowledge-based approach for
595 interpreting genome-wide expression profiles. *Proc. Natl. Acad. Sci.* **102**, 15545–15550 (2005).
596 33. Liberzon, A. *et al.* The Molecular Signatures Database Hallmark Gene Set Collection. *Cell Syst.* **1**,
597 417–425 (2015).
598 34. Yadav, N. *et al.* Oxidative phosphorylation-dependent regulation of cancer cell apoptosis in
599 response to anticancer agents. *Cell Death Dis.* **6**, e1969–e1969 (2015).
600 35. Creighton, C. J. *et al.* Residual breast cancers after conventional therapy display mesenchymal as
601 well as tumor-initiating features. *Proc. Natl. Acad. Sci.* **106**, 13820–13825 (2009).
602 36. Jing, X. *et al.* Role of hypoxia in cancer therapy by regulating the tumor microenvironment. *Mol.*
603 *Cancer* **18**, 157 (2019).
604 37. Jeter, C. R. *et al.* NANOG promotes cancer stem cell characteristics and prostate cancer
605 resistance to androgen deprivation. *Oncogene* **30**, 3833–3845 (2011).
606 38. Kumar, S. M. *et al.* Acquired cancer stem cell phenotypes through Oct4-mediated
607 dedifferentiation. *Oncogene* **31**, 4898–4911 (2012).
608 39. Leis, O. *et al.* Sox2 expression in breast tumours and activation in breast cancer stem cells.
609 *Oncogene* **31**, 1354–1365 (2012).
610 40. Fuerer, C. & Nusse, R. Lentiviral Vectors to Probe and Manipulate the Wnt Signaling Pathway.
611 *PLoS One* **5**, e9370 (2010).
612 41. Horst, D. *et al.* Differential WNT Activity in Colorectal Cancer Confers Limited Tumorigenic
613 Potential and Is Regulated by MAPK Signaling. *Cancer Res.* **72**, 1547–1556 (2012).
614 42. Takebe, N. *et al.* Targeting Notch, Hedgehog, and Wnt pathways in cancer stem cells: clinical
615 update. *Nat. Rev. Clin. Oncol.* **12**, 445–464 (2015).
616 43. Jin, W. Role of JAK/STAT3 Signaling in the Regulation of Metastasis, the Transition of Cancer Stem
617 Cells, and Chemoresistance of Cancer by Epithelial–Mesenchymal Transition. *Cells* **9**, 217 (2020).
618 44. Liu, S., Ren, J. & ten Dijke, P. Targeting TGFβ signal transduction for cancer therapy. *Signal*
619 *Transduct. Target. Ther.* **6**, 8 (2021).
620 45. Ma, B. & Hottiger, M. O. Crosstalk between Wnt/β-Catenin and NF-κB Signaling Pathway during
621 Inflammation. *Front. Immunol.* **7**, (2016).
622 46. Niehrs, C. & Acebron, S. P. Mitotic and mitogenic Wnt signalling. *EMBO J.* **31**, 2705–2713 (2012).
623 47. Dhimolea, E. *et al.* An Embryonic Diapause-like Adaptation with Suppressed Myc Activity Enables
624 Tumor Treatment Persistence. *Cancer Cell* **39**, 240-256.e11 (2021).
625 48. Ramponi, V. *et al.* Persister cancer cells are characterized by H4K20me3 heterochromatin that
626 defines a low inflammatory profile. *bioRxiv* (2024) doi:10.1101/2024.01.26.577389.
627 49. Torres, V. I., Godoy, J. A. & Inestrosa, N. C. Modulating Wnt signaling at the root: Porcupine and

628 Wnt acylation. *Pharmacol. Ther.* **198**, 34–45 (2019).
629 50. Hofmann, K. A superfamily of membrane-bound O -acyltransferases with implications for Wnt
630 signaling. *Trends Biochem. Sci.* **25**, 111–112 (2000).
631 51. Zhong, Z. *et al.* PORCN inhibition synergizes with PI3K/mTOR inhibition in Wnt-addicted cancers.
632 *Oncogene* **38**, 6662–6677 (2019).
633 52. Madan, B. *et al.* Wnt addiction of genetically defined cancers reversed by PORCN inhibition.
634 *Oncogene* **35**, 2197–2207 (2016).
635 53. García-Reyes, B. *et al.* Discovery of Inhibitor of Wnt Production 2 (IWP-2) and Related
636 Compounds As Selective ATP-Competitive Inhibitors of Casein Kinase 1 (CK1) δ/ε. *J. Med. Chem.*
637 **61**, 4087–4102 (2018).
638 54. Alfarouk, K. O. *et al.* Resistance to cancer chemotherapy: failure in drug response from ADME to
639 P-gp. *Cancer Cell Int.* **15**, 71 (2015).
640 55. Garg, H., Suri, P., Gupta, J. C., Talwar, G. P. & Dubey, S. Survivin: a unique target for tumor
641 therapy. *Cancer Cell Int.* **16**, 49 (2016).
642 56. Rodon, J. *et al.* Phase 1 study of single-agent WNT974, a first-in-class Porcupine inhibitor, in
643 patients with advanced solid tumours. *Br. J. Cancer* **125**, 28–37 (2021).
644 57. Tabernero, J. *et al.* A Phase Ib/II Study of WNT974 + Encorafenib + Cetuximab in Patients With
645 BRAF V600E -Mutant KRAS Wild-Type Metastatic Colorectal Cancer. *Oncologist* **28**, 230–238
646 (2023).
647 58. Moisan, F. *et al.* Enhancement of paclitaxel and carboplatin therapies by CCL2 blockade in
648 ovarian cancers. *Mol. Oncol.* **8**, 1231–1239 (2014).
649 59. MABUCHI MIYUKI. Systematic Trial for Evaluating Docetaxel in a Human Prostate Cancer Cell
650 DU145 Xenograft Model. *Anticancer Res.* **37**, 1665–1676 (2017).
651 60. Yun, E.-J. *et al.* Targeting Cancer Stem Cells in Castration-Resistant Prostate Cancer. *Clin. Cancer*
652 *Res.* **22**, 670–679 (2016).
653 61. Abreu de Oliveira, W. A. *et al.* Wnt/β-Catenin Inhibition Disrupts Carboplatin Resistance in
654 Isogenic Models of Triple-Negative Breast Cancer. *Front. Oncol.* **11**, (2021).
655 62. Matikas, A. *et al.* Dynamic evaluation of the immune infiltrate and immune function genes as
656 predictive markers for neoadjuvant chemotherapy in hormone receptor positive, HER2 negative
657 breast cancer. *Oncoimmunology* **7**, e1466017 (2018).
658 63. Kimbung, S. *et al.* Assessment of early response biomarkers in relation to long-term survival in
659 patients with HER2-negative breast cancer receiving neoadjuvant chemotherapy plus
660 bevacizumab: Results from the Phase II PROMIX trial. *Int. J. Cancer* **142**, 618–628 (2018).
661 64. Tempfer, C. Basal-like molecular subtype and HER4 up-regulation and response to neoadjuvant
662 chemotherapy in breast cancer. *Oncol. Rep.* (2011) doi:10.3892/or.2011.1392.
663 65. Driehuis, E., Kretzschmar, K. & Clevers, H. Establishment of patient-derived cancer organoids for
664 drug-screening applications. *Nat. Protoc.* **15**, 3380–3409 (2020).
665 66. Wensink, G. E. *et al.* Patient-derived organoids as a predictive biomarker for treatment response
666 in cancer patients. *npj Precis. Oncol.* **5**, 30 (2021).
667 67. Sachs, N. *et al.* A Living Biobank of Breast Cancer Organoids Captures Disease Heterogeneity. *Cell*
668 **172**, 373-386.e10 (2018).
669 68. Shang, S. *et al.* Chemotherapy-Induced Distal Enhancers Drive Transcriptional Programs to
670 Maintain the Chemoresistant State in Ovarian Cancer. *Cancer Res.* **79**, 4599–4611 (2019).
671 69. Wang, L. *et al.* Chromatin accessibility regulates chemotherapy-induced dormancy and
672 reactivation. *Mol. Ther. - Nucleic Acids* **26**, 269–279 (2021).
673 70. Chera, S. *et al.* Apoptotic Cells Provide an Unexpected Source of Wnt3 Signaling to Drive Hydra
674 Head Regeneration. *Dev. Cell* **17**, 279–289 (2009).
675 71. Wang, W. *et al.* ABL1-dependent OTULIN phosphorylation promotes genotoxic Wnt/β-catenin

676 activation to enhance drug resistance in breast cancers. *Nat. Commun.* **11**, 3965 (2020).
677 72. Ince, T. A. *et al.* Characterization of twenty-five ovarian tumour cell lines that phenocopy primary
678 tumours. *Nat. Commun.* **6**, 7419 (2015).
679 73. Bolger, A. M., Lohse, M. & Usadel, B. Trimmomatic: a flexible trimmer for Illumina sequence data.
680 *Bioinformatics* **30**, 2114–2120 (2014).
681 74. Dobin, A. *et al.* STAR: ultrafast universal RNA-seq aligner. *Bioinformatics* **29**, 15–21 (2013).
682 75. Liao, Y., Smyth, G. K. & Shi, W. featureCounts: an efficient general purpose program for assigning
683 sequence reads to genomic features. *Bioinformatics* **30**, 923–930 (2014).
684 76. Love, M. I., Huber, W. & Anders, S. Moderated estimation of fold change and dispersion for RNA-
685 seq data with DESeq2. *Genome Biol.* **15**, 550 (2014).
686 77. Desmedt, C. *et al.* Biological Processes Associated with Breast Cancer Clinical Outcome Depend
687 on the Molecular Subtypes. *Clin. Cancer Res.* **14**, 5158–5165 (2008).
688 78. R Core Team. R: A language and environment for statistical computing. (2021).
689

690

691 **AUTHOR CONTRIBUTIONS**

692 YEL, WO, and FL conceived and designed the study. WO partially carried out flow cytometry experiments,
693 RT-qPCR experiments, analysis of publicly available datasets. AP performed all bioinformatic and
694 biostatistical analyses under the supervision of FR and CD. AQ partially carried out flow cytometry
695 experiments, western blot analysis, RT-qPCR experiments, and *in vivo* experiments. FR provided critical
696 input for the bulk transcriptomic analysis under supervision of and in consultation with CD. PA participated
697 in library preparations for mRNA-seq samples and provided input in experimental design. CL and WDW
698 provided aid in the *in vivo* experiments under supervision of SS and DA. LM provided aid for the culturing
699 and maintenance of patient derived organoid (PDO) models. SH provided input and feedback into
700 experimental design under supervision of AB. SM generated the *in vitro* cell line, PDC-BRC-101. AdJS
701 provided critical input in experimental design and assisted in the generation of several fluorescent reporter
702 cell lines. MB provided input in the *in vivo* experimental design. SJS provided critical input in human patient
703 dataset analysis. CS provided the PDO models. AB provided critical input for experimental design. DA
704 provided critical input in *in vivo* data analysis. YEL carried out the remainder of the experimental work.
705 Data analysis and figure preparation were performed by YEL and WO and reviewed by FL. The manuscript
706 was written by YEL and FL and reviewed and approved by all authors. FL secured funding and supervised
707 and guided experimental work and manuscript preparation.
708
709

710 **ACKNOWLEDGEMENTS**

711 We are grateful to the KU Leuven FACS core team for providing the facility. We also thank the KU Leuven
712 Genomics Core (http://genomicscore.be) for RNA sequencing, and data processing. We also thank the KU
713 Leuven TRACE core and the MOSAIC core for help in *in vivo* experimental design and animal imaging. The
714 authors would like to extend their gratitude to the FWO Research Foundation – Flanders for the Ph.D.
715 fellowships awarded to P.A. (11M7822N). AdJS was supported by PhD Emmanuel van der Schueren (EvdS)
716 fellowship granted by Kom Op Tegen Kanker (KOTK) and a Postdoctoral Mandate (PDM) granted by KU
717 Leuven. The Lluis Lab is financed by the FWO Research Project Grants G091521N (AB, DA, FLL), G073622N
718 (FLL), and the C1 KU Leuven internal grant C14/21/115 (FLL).
719
720

721 **MATERIALS AND METHODS**

722 **Ethics declaration**

723 All xenograft animal experiments performed were approved by the Ethics Committee at KU Leuven
724 University under the ethical approval codes P055/2022 and P016/2023.
725
726 Patient derived organoid (PDO) models used in this study were established from freshly resected tumor
727 tissues obtained from TNBC patients at the Antoni van Leeuwenhoek Hospital. The study was approved by
728 the institutional review board (NKI-B17PRE) and the subjects provided informed consent.
729
730 All cell lines used in this study are approved for use by the Ethics Committee at the KU Leuven University
731 Biobank under the code S65166.
732

733 **TNBC cell line culture**

734 MDA-MB-231 (ATCC-HTB-26) and MDA-MB-468 (ATCC-HTB-132) were maintained in DMEM high glucose
735 (Gibco, 41965039) supplemented with 10% (v/v) fetal bovine serum, 1mM sodium pyruvate (Gibco,
736 11140035), 100µg/mL penicillin-streptomycin (Gibco, 15140163), and 0.01mM 2-mercapthoethanol
737 (Gibco, 31350010).
738
739 PDC-BRC-101 cell line (PDX-derived cell line) was obtained from collaborators, Daniela Anibali and Stijn
740 Moens (Amant Lab – Gynecological Oncology) – KU Leuven and maintained in OCMI media[72] composed of
741 a composed of 1:1 mixture of Medium199 (Gibco, 31150022) and DMEM F-12 (Gibco, 11320074)
742 supplemented with 10% (v/v) fetal bovine serum, 100µg/mL penicillin-streptomycin, 20µg/mL insulin
743 (Sigma/Merck, I9278), 25ng/mL cholera toxin subunit B (Sigma/Merck, C9903-.5MG), 0.5µg/mL
744 hydrocortisone (Sigma/Merck, H0888-1G), and 10ng/mL epidermal growth factor (Stem Cell Technologies,
745 78006.1).
746
747 All cell lines were cultured in 84mm x 20mm (D x H) tissue-culture treated dishes at 37°C and 5% CO_2 and
748 maintained at 70-80% confluency. For cell line passaging and plating, 1X phosphate-buffered saline (Gibco,
749 10010-015) was used as a washing solution followed by dissociation using 0.25% trypsin-EDTA (Gibco,
750 25200-056) and cell-pelleting by centrifugation for 4 minutes at 300G (0.3rcf). Cells were counted
751 manually via the BRAND counting chamber Neubauer improved (Sigma Aldrich/Merck, BR717810-1EA)
752 under a 10X objective lens using a Leica DMi inverted microscope. The same microscope, equipped with a
753 2.5 Megapixel HD Microscope Camera Leica MC120 HC, was used to obtain images of cultured cancer cell
754 lines. Unless specified otherwise, cancer cell lines were plated according to the following seeding
755 densities: $7.3\ x\ 10^3\ \frac{cells}{cm^2}$ and $10.5\ x\ 10^3\ \frac{cells}{cm^2}$ (MDA-MB-231 and MDA-MB-468/PDC-BRC-101,
756 respectively).
757

758 **Chemotherapeutic treatment of TNBC cell lines and PDO models**

759 Cell lines were treated with increasing concentrations of docetaxel (Taxotere, 0–144 nM) and carboplatin
760 (Carbosin, 0–1600 µM) for 72h. Cell metabolic activity, reflecting cell-number and -viability) was assessed
761 using the MTT [Thiazolyl Blue Tetrazolium Bromide] assay (Sigma/Merck, M5655-500mg) according to
762 manufacturer's instructions and sigmoidal dose-response curves were generated to calculate the mean

763 IC50 values of each drug that were used in the subsequent study. Chemotherapeutic agents were obtained
764 from the pharmacy of Universitair Ziekenhuis (UZ) Leuven.
765
766 **Lentiviral particle production and transduction**
767 Lentiviruses were produced according to the RNAi Consortium (TRC) protocol available from the Broad
768 Institute (https:// portals.broadinstitute.org/gpp/public/resources/protocols). In brief, $7\,x\,10^5$
769 HEK-293T cells were seeded per well in 6-well plates and transfected the following day with 750 µg pCMV-
770 dR8.91, 250 µg pCMV-VSV-G, and 1 µg of the specific lentiviral plasmid/construct using FugeneHD
771 (Promega, E2311) in Optimem (Gibco, 31985070). One day after, the culture medium was refreshed. The
772 same day, lentivirus-recipient cells were plated in 6-well plates at their respective concentrations (see cell
773 line culture). Lentivirus-containing medium was collected from HEK293T cells 48h and 72h post-
774 transfection and added to recipient cancer cells after filtration using a 0.45 µM filter (VWR-Corning,
775 431220). 48h post infection, recipient cancer cells were washed thoroughly with PBS, medium refreshed,
776 and the appropriate selection antibiotics applied until selection process was completed.
777
778 Wnt-transcriptional reporters, TOPGFP (7xTOP-GFP), TOPFLASH (7xTcf-FFluc), and mCherry-TOPGFP
779 (7xTOP-GFP.mC) were obtained from Addgene (#35489, #24308, and #35491, respectively). Wnt-
780 transcriptional reporter dTOPGFP was gifted to us from the Moon lab University of (Washington – USA).
781
782 For PORCN shRNA mediated silencing, we used the MISSION® Lentiviral shRNA (Sigma Aldrich/Merck,
783 SHCLNG – clones, TCRN000153848 and TCRN000157366) and the MISSION pLKO.1-puro Non-Target
784 shRNA Control Plasmid DNA (SHC016-1EA) as a negative control in experiments.
785
786 **Real-Time Quantitative Polymerase Chain Reaction and Gene Expression Analysis**
787 For RT-qPCR, total RNA was extracted (from TNBC cell lines or cryopreserved tumor tissue) using the
788 GenElute mammalian total RNA miniprep kit (Sigma/Merck, RTN350-1KT) according to manufacturer's
789 instructions with an additional step of DNA digestion using the On-Column DNAse I digestion set according
790 to manufacturer's instructions (Sigma/Merck, DNASE70). cDNA was synthesized from 500 ng of total RNA
791 using the BIORAD iScript cDNA cDNA synthesis kit (BIORAD, CAT#1708891), according to manufacturer's
792 instructions. Quantitative real-time PCR reactions were set up in technical triplicates with Platinum SYBR
793 Green qPCR SuperMix-UDG (Invitrogen, 11733-046) on a ViiA7 Real-Time PCR System (Thermo-Scientific).
794 Expression levels were normalized to two housekeeping genes (HK) RPL19 and GAPDH to determine ΔCT
795 values. Statistical testing of differences in expression levels between samples was carried out based on
796 relative-expression values ($2^{-\Delta CT}$). In some figures, gene expression values are represented as fold-
797 change for convenience of interpretation, although statistical testing was performed on relative expression
798 values ($2^{-\Delta CT}$).
799
800 **SDS-PAGE and Western Blot analysis**
801 TNBC cell lines were washed with PBS and collected/pelleted by centrifugation. Whole cell lysates were
802 obtained via mechanical lysis using a needle (VWR-TERUMO, AN2138R1) and RIPA cell lysis buffer
803 (Sigma/Merck, R0278-50mL) supplemented with a cocktail of 1:100 phosphatase inhibitors cocktail 2 and
804 3 (Sigma/Merck, P5726-1ML and P0044-1ML, respectively) and 1:100 protease inhibitor cocktail
805 (Sigma/Merck, 11873580001). Samples were placed on a rotation wheel for a minimum of 30 minutes at

806 4 °C after which they were centrifuged at 16,000x g for 10 minutes at 4 °C. The supernatant from the
807 lysates was collected and protein concentration was determined using the Bradford Assay (Biorad,
808 5000006). For SDS-PAGE 20 mg of protein were mixed with 4x Laemmli buffer (240 mM Tris/HCL pH 6.8,
809 8% SDS, 0.04% bromophenol blue, 5% 2-mercaptoethanol, 40% glycerol) and denatured for 5 minutes at
810 95°C prior to electrophoretic protein separation. Resolved protein extracts were transferred to PVDF
811 membranes (BIORAD, 162-0177). Transfer success was assessed with Ponceau S solution, and membranes
812 were blocked with 5% non-fat milk or 5% BSA in TBS-T (0.1% Tween-20®) for 60 minutes. After blocking,
813 membranes were incubated with primary antibodies at 4°C overnight. The day after, membranes were
814 washed 3 times with PBS-T for 10 minutes and incubated with secondary HRP-conjugated antibodies.
815 Immunolabeled proteins were detected with Supersignal West Pico chemiluminescent kit (Fisher
816 Scientific, 34077) on autoradiography film (Santa Cruz, SC-201697). The primary antibodies used were
817 active rabbit anti-non-phosphorylated β-catenin (CellSignaling Technologies, #19807S), rabbit anti-PORCN
818 (Novus Biologicals, NBP1-59677), and rabbit anti-WNT2b (Abcam, ab178418). Mouse anti-β-Actin (Santa
819 Cruz Biotechnology; sc-47778) was used as a loading control.
820
821 **Flow Cytometry**
822 For Wnt-activation assessment, cells were washed with PBS and collected/pelleted by centrifugation. Cells
823 were resuspended in PBS2%FBS, counterstained with 5µg of 4',6-diamidino-2- phenylindole (DAPI – 1:1)
824 (Sigma/Merck, D9542-10mg) to eliminate dead cells before running through the flow cytometer. Cell lines
825 lacking any of the previously described Wnt-transcriptional reporters were used as gating controls.
826
827 For ALDH activity assay, cells were washed with PBS and collected/pelleted by centrifugation. Cells were
828 stained using the AldeRed ALDH detection assay (Sigma/Merck, SRC150) according to manufacturer
829 instructions. Cells were counterstained with 5µg of DAPI (1:1) to eliminate dead cells before running
830 through the flow cytometer.
831
832 For Annexin V apoptosis analysis, cells were washed with PBS and collected/pelleted by centrifugation.
833 Cells were resuspended in 1x Annexin V binding buffer (BD Pharmigen, 51-66121E) and incubated at room
834 temperature in the dark for 15 minutes with APC-conjugated Annexin V (Thermo-eBioscience,
835 BMS306APC-100). After incubation, cells were diluted in 1X binding buffer supplemented with 100 nM of
836 DAPI before running through the flow cytometer. Unstained and single-stained (Annexin V-only or DAPI-
837 only stained) cells were used as gating controls.
838
839 To obtain chemotherapy-induced Wnt^{High} and Wnt^{Low} cells, cells were washed with PBS and
840 collected/pelleted by centrifugation. Cells were resuspended in PBS4%FBS, counterstained with 5µg of
841 DAPI (1:1) to eliminate dead cells before running through the SONY MA900 Multi-Application Cell Sorter.
842 Depending on the application, $2 - 3\ x\ 10^5$cells were sorted (based on their GFP expression) into 1.5mL
843 Eppendorf tubs (with 300µl of PBS4%FBS) and either used for RNA-extraction and gene expression analysis
844 or for re-culturing.
845
846 For immunostaining of active- (non-phosphorylated) β-catenin, cells were washed with PBS and
847 collected/pelleted by centrifugation. Cells were fixed with ice-cold 70% Ethanol. After which samples were
848 with PBS2%FBS and blocked with 5% donkey serum (in PBS) at room temperature for 30-60 minutes. Cells
849 were re-pelleted by centrifugation, washed with PBS2%FBS and incubated with active rabbit anti-non-

850 phosphorylated β-catenin antibody at room temperature for 60 minutes. Cells were re-pelleted by
851 centrifugation, washed with PBS2%FBS and incubated with a conjugated secondary (donkey anti-rabbit –
852 Alexa-647 – Thermo-Life tech, A31573) in the dark at room temperature for 30 minutes. Cells were re-
853 pelleted by centrifugation, washed with PBS2%FBS and counterstained with 5µg of DAPI (1:1) before
854 running through the flow cytometer. Unstained and single-stained (secondary antibody-only stained) cells
855 were used as gaiting controls.
856
857 Unless specified otherwise, all data were collected on a BD FACS Canto II at the KU Leuven Flow Cytometry
858 Core and analyzed using FlowJo v.10.6.2.
859
860 **Conditioned media and co-culture analysis**
861 Conditioned media (CM) was collected from TNBC cell lines recovering from chemotherapy treatment (5
862 days of treatment and 1 week of recovery) and filtered using a 0.45µM filter to ensure removing cell-
863 debris. Filtered CM as concentrated 20x (20mL to 1mL) using Vivaspin centrifugal concentrator column
864 with a molecular weight cutoff of 50kDa (Sigma Aldrich, Z614645-12EA). Filtered media was centrifuged
865 for 45 minutes at 4°C. Concentrated CM was added to chemo-naïve TNBC cell lines for 48h in a 1:1 dilution
866 (Concentrated CM:basal culture cancer media) and Wnt-activation levels were evaluated using FACS.
867
868 For co-culture experiments, MDA-MB-231 cell line was treated with either chemotherapeutic agent for
869 72h after which treatment was stopped and an equal number of chemo-naïve MDA-MB-231-TGP.mC cells
870 was plated in the same dish and cultured in basal culture cancer media. After 72h of co-culture, Wnt-
871 activation levels in the MDA-MB-231-TGP.mC cell line was evaluated using FACS.
872
873 **Cell line derived xenograft establishment and *in vivo* live imaging analysis**
874 $1\ x\ 10^6$ MDA-MB-231 TOPFLASH cells were engrafted subcutaneously (1:1 PBS: growth-factor reduced
875 Matrigel) into the right flank of female NMRI-Foxn1 mice (4-6 weeks old) to form a solid tumor. Upon
876 observation of visible/palpable solid growth, tumor volumes were measured using digital calipers (and
877 calculated as $L\ x\ W\ x\ \frac{\pi}{6}$; L: length and W: width). Animals were randomly assigned to one of three (or six)
878 treatment groups (n = 7-8 mice per group) with an average tumor volume of 150mm^3 per group. Docetaxel
879 (15mg/kg) and Carboplatin (100mg/kg) were administered via intraperitoneal (IP) injection once weekly
880 (1 cycle) for a total of three cycles. LGK-974 (2mg/kg) was administered daily via oral gavage for a total of
881 3 cycles (3 weeks). For assessment of Wnt-activation dynamics, animals were subjected to live-
882 bioluminescent imaging before-, 24 h-, 48h-, and 72h- after chemotherapeutic administration. For live-
883 bioluminescent imaging, animals were injected (IP) with the luciferase substrate D-luciferin (200µL of
884 15mg/ml - assuming an average animal weight of 24-26gr) (Perkin Elmer, 122799) and incubated for 10
885 minutes at room temperature before images were taken using IVIS Spectrum In Vivo Imaging System
886 (Perkin Elmer). Wnt-activation signal was calculated as the bioluminescent signal captured by the IVIS
887 Spectrum normalized to the tumor volume recorded per animal. Analysis of bioluminescent images was
888 performed via the Aura software v.4.0.0. Tumor volume was recorded every 48h and body weight was
889 closely monitored throughout the treatment course and recorded every 72-96h using an automatic scale.
890 All animals were euthanized at the end of the treatment course and tumors (when available) were
891 resected/collected for downstream analyses.
892
893

894 **RECIST Analysis**
895 RECIST analysis was performed using tumor volumes measured and recorded (as described previously) at
896 the onset of treatment and at the end of treatment (day of sacrifice). Relative tumor volume (RTV) was
897 calculated by dividing the recorded volume at the end of treatment by the recorded volume at the onset
898 of treatment. Response to therapy was based on the RECIST-based criterion: Complete response (CR),
899 Partial response (PR), Stable disease (SD), and Progressive disease (PD); CR: RTV = 0, PR: 0 < RTV ≤ 0.657,
900 SD: 0.657 < RTV ≤ 1.728, PD: RTV > 1.728.
901
902 **Tumorsphere Formation Assay**
903 Cells were washed with PBS and collected/pelleted by centrifugation. Cells were resuspended in
904 PBS4%FBS, counterstained with 5µg of DAPI (1:1) to eliminate dead cells before running through the SONY
905 MA900 Multi-Application Cell Sorter. $1\ x\ 10^3$single cells were sorted (based on their GFP expression)
906 directly in ultra-low attachment 6-well plates (Fisher-Corning, 10154431) cultured in serum-free
907 tumorsphere assay medium composed of DMEM/F12 (Gibco, 11320074), 1X B27 (Thermo-Scientific,
908 12587010), 10ng/mL basic fibroblast growth factor (bFGF) (Peprotech, 100-18b), 20ng/mL EGF (Peprotech,
909 AF-100-15), and 2% growth-factor reduced Matrigel (Corning, 734-0268). Sorted cells were allowed
910 fourteen days to grow, at the end of which, spheres were collected and centrifuged at 50g for 10minutes,
911 resuspended gently, and transferred to 96-well plates (Fisher-Falcon,353072). Plates were briefly
912 centrifuged at 50g for an additional 1 minutes to pull down larger spheroid (>60 µm) which were counted
913 under a microscope (10X) using a tally counter.
914
915 **Next-Generation mRNA Sequencing**
916 Total RNA was obtained from cells using the GenElute mammalian total RNA miniprep kit (Sigma, RTN350-
917 1KT). RNA-sequencing (RNA-seq) libraries were prepared using 750 ng of total RNA using the KAPA
918 stranded mRNAseq kit (Roche, 8098123702) according to the manufacturer's specifications. 100 nM of
919 KAPA-single index adapters (Roche, KK8702) were added to the A-tailed cDNA and the libraries underwent
920 10 cycles of amplification. Agentcourt AMPure XP beads (Beckman Coulter, A63880) were used for the 1X
921 library clean-up. The fragment size of the libraries was assessed using the Agilent Bioanalyzer 2100 with
922 the High Sensitivity DNA kit (Agilent, 5067-4626). The concentration of the libraries was measured by the
923 High Sensitivity QuBit kit (Invitrogen, Q33230). Each library was diluted to 4 nM and pooled for single-end
924 50-bp sequencing on an Illumina Hiseq4000 with 20 – 27 million reads per sample (22 million reads on
925 average).
926
927 **Bulk mRNA-sequencing analysis**
928 FASTQ files generated from the sequencing (Sequencing run Fig. 1 and Fig. 3) were sent for downstream
929 processing. Adapters were trimmed using Trimmomatic[73] v0.39 and the trimmed FASTQ file was aligned
930 to the GRCh38 genome (hg38) using the STAR aligner[74] v2.7.10. Gene counts, gene annotation and sample
931 read characteristics were obtained by applying standard filters within featureCounts[75] from the subread
932 package v2.0.3. Gene counts were then normalized using the variance stabilizing transformation (VST). Z-
933 scores used to describe the gene expression distribution across samples were calculated using median
934 absolute deviation whole the heatmaps comparing z-scores between samples were created using
935 pheatmap v1.0.12. Differential gene expression analysis was performed using DESeq2[76] and batch effects
936 were accounted for in the (Wnt^{High} vs. Wnt^{Low} cohort). Volcano plots were created using EnhancedVolcano
937 v1.18.0 using custom settings of FCcutoff = 0.6 and pCutoff = 0.05. Gene set variation analysis was

938 performed using GSVA v1.48.3. Signature scores for the Caspase 3/Apoptosis[77] and diapause/DTP
939 signatures (Supplementary Table 4) were calculated after the gene counts were transformed using both
940 log2(x) +1 and VST methods. Box plots comparing the signature score(s) distribution between Wnt^{High} and
941 Wnt^{Low} samples between treatment conditions were created using ggplot2 v3.4.3. Forest plots for
942 regression analysis were created using forestplot v3.1.3. Analyses following the gene count extraction
943 were all performed in R[78] v4.3.0.
944
945 **Functional Enrichment Analysis of publicly available datasets**
946 Datasets GSE87455 and GSE21974 were downloaded from the GeneExpression Omnibus and ArrayExpress
947 public repositories, respectively. Differentially expressed genes with |log2(fold-change)| >1 and p-value <
948 0.05 were obtained using limma (v3.26.8) R package in R (v4.02) and by using the limma method on
949 NetworkAnalyst (39). Differentially expressed genes were ranked by fold-change for Gene Set Enrichment
950 Analysis (GSEA v4.1.0) using the weighted enrichment statistic for Hallmark and KEGG gene sets from the
951 human MSigDB database. The statistical significance threshold was set at FDR<0.1 or ($p<0.5 \wedge FDR<0.25$)
952
953 **Patient derived organoid culture, treatment, and analysis**
954 R1-IDC113 and R2-IDC159A PDO lines were gifted by our collaborator, Laboratory of Colinda Scheele – VIB-
955 KU Leuven. Both PDO lines were maintained in growth factor reduced type 2 Cultrex (Biotechne/R&D
956 Systems, 3533-010-02) with phenol red-free DMEM/F-12, HEPES (Gibco, 11039021) supplemented with
957 10mM Nicotinamide (Sigma/Merck, N0636-100G), 1.25mM N-acetyl-L-cystine (Sigma/Merck, A9165-5G),
958 500ng/mL Hydrocortisone, 100nM β-estradiol (E8875-250MG), 500nM SB202190 (Stem Cell Technologies,
959 72632), 500nM A83-01 (Stem Cell Technologies, 72022), 5uM Y-27632 (Stem Cell Technologies, 72304),
960 50µg/mL Primocin (Invivogen, ant-pm-05), 10µM Forskolin (Sigma/Merck, F3917-10MG), 1X B27 (50X –
961 ThermoFisher Scientific, 17504044), 100ng/mL r-Noggin (Stem Cell Technologies, 78060), 5ng/mL FGF-10
962 (Stem Cell Technologies, 78037), 37.5 ng/mL Heregulin B-1 (Peprotech, 100-03), 5ng/mL EGF, 5ng/mL FGF-
963 7 (Peprotech, 100-19), and 100µg/mL penicillin-streptomycin.
964
965 Both PDO lines were cultured in 24 well cell culture microplates – 22 mm x 20 (D x H) – at 37°C and 5%
966 CO_2 and maintained at 70-80% confluency. For passaging and plating, (ice-cold) 1X phosphate-buffered
967 saline (Gibco, 10010-015) was used to wash and dissociate the BME followed by single cell enzymatic
968 dissociation using 0.05% trypsin-EDTA (Gibco, 25200-056) and cell-pelleting by centrifugation for 5
969 minutes at 1500 rpm (4°C). Cells were counted manually via the BRAND counting chamber Neubauer
970 improved (Sigma Aldrich/Merck, BR717810-1EA) under a 10X objective lens using a Leica DMi inverted
971 microscope. The same microscope, equipped with a 2,5 Megapixel HD Microscope Camera Leica MC120
972 HC, was used to obtain images of cultured PDO-lines. Unless specified otherwise, both PDO models were
973 plated according to the following seeding density: $5.9\ x\ 10^2\ \frac{cells}{mm^2}$
974
975 To determine working chemotherapy drug concentrations, PDO lines were treated with increasing
976 concentrations of docetaxel (Taxotere, 0.0625–512 nM) and carboplatin (Carbosin, 0 – 1600 µM) for 96h.
977 Cell metabolic activity, reflecting cell-number and –viability was assessed using the CellTiter-Glo® 3D Cell
978 Viability Assay (Promega, G9682) and sigmoidal dose-response curves were generated to calculate the
979 mean IC50 values of each drug that were used in the subsequent study. Chemotherapeutic agents were
980 obtained from the pharmacy of Universitair Ziekenhuis (UZ) Leuven.

Statistical Analysis

All data were analyzed using GraphPad Prism (v8.0.1), except for mRNA-sequencing derived data and transcriptomic datasets. Unless otherwise specified, comparisons between two groups were tested for statistical significance using Unpaired t-tests. Comparisons between multiple groups were performed using a One-way analysis of variance (ANOVA). Comparisons between multiple groups across multiple time points were performed using Two-way ANOVA. All statistical testing was corrected for multiple comparisons, using the Holm-Sidak method when comparing samples based on experimental design. For the reader's convenience, all statistical tests and sample sizes are indicated in the figure legends.

For mRNA-sequencing derived data, regression analysis was performed to observe associations between outcomes (in-house gene signature scores/GSVA signature scores) and independent co-variate (Wnt^{High} vs. Wnt^{Low}) per treatment condition (CAR or DOC or UNT) using lqmm v.1.5.8 and quantreg v5.97 while accounting for batch effects.

Schematic Illustrations and artwork

All schematic illustrations were created using Biorender.com

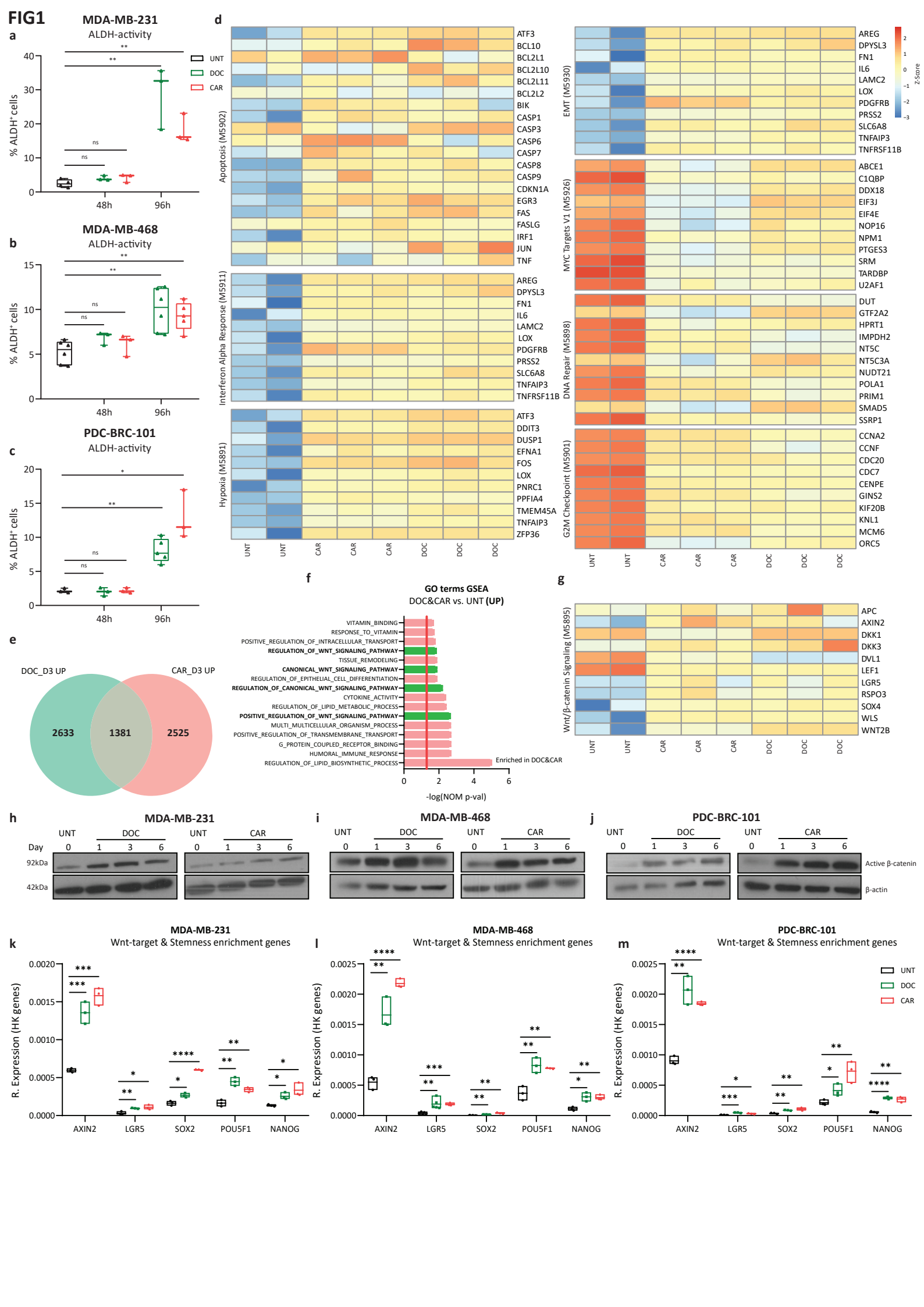
FIG1
a
MDA-MB-231
ALDH-activity
% ALDH+ cells
UNT
DOC
CAR
48h
96h
b
MDA-MB-468
ALDH-activity
c
PDC-BRC-101
ALDH-activity
d
Apoptosis (M5902)
Interferon Alpha Response (M5911)
Hypoxia (M5891)
EMT (M5930)
MYC Targets V1 (M5926)
DNA Repair (M5898)
G2M Checkpoint (M5901)
Z-Score
e
DOC_D3 UP
CAR_D3 UP
2633
1381
2525
f
GO terms GSEA
DOC&CAR vs. UNT (UP)
Enriched in DOC&CAR
-log(NOM p-val)
g
Wnt/β-catenin Signaling (M5895)
h
MDA-MB-231
Day
92kDa
42kDa
i
MDA-MB-468
j
PDC-BRC-101
Active β-catenin
β-actin
k
MDA-MB-231
Wnt-target & Stemness enrichment genes
R. Expression (HK genes)
AXIN2
LGR5
SOX2
POU5F1
NANOG
l
MDA-MB-468
m
PDC-BRC-101

Figure 1: Wnt-transcriptional activation precedes drug-tolerant cell(s) enrichment upon chemotherapeutic treatment

a-c) Flow cytometry analysis displaying %ALDH$^+$ cells of MDA-MB-231 (top), MDA-MB-468 (middle), and PDC-BRC-101 (bottom) cell lines treated with DOC (4.5nM) or CAR (35uM, 25uM, 35uM for each cell line, respectively) for 48h and 96h. Multiple t-tests corrected for multiple comparisons using the Holms-Sidak method (n = 3 independent experiments). All data points shown from min. to max. (box and whiskers). **d)** Normalized gene expression heatmaps displaying (≈12-20) selected genes (based on DEGs predicting each representative process and/or hallmark) representing different processes and signaling cascades deregulated (relative to UNT cells) in MDA-MB-231 cell line treated with DOC or CAR for 72h. The processes (and subsequent genes selected to represent every process) shown in panel **d** were based on enriched gene sets from Hallmarks databases analyzed by one-tailed GSEA ranked by Normalized Enrichment Score (NES) - Supplementary Fig. S1j, k. **e)** Venn diagram indicating commonly upregulated (1381) genes between DOC (2633) and CAR (2525) treatment (vs. UNT). **f)** Enriched processes from Gene Ontology (GO) terms databases analyzed by one-tailed GSEA ranked by a positive NES and based on commonly upregulated genes between DOC and CAR treatment. Red line indicates significance threshold value, (-log(NOM p-val) = 1.3) and highlighted bars indicate GO terms linked to Wnt/β-catenin signaling regulation. **g)** Normalized gene counts heatmap displaying (11) selected genes representing Wnt/β-catenin signaling in MDA-MB-231 cell line treated with DOC and CAR for 72h. Genes selected for heatmap **g** were based on Wnt/β-catenin signaling Hallmark – GSEA. Data used to generate panels **d-g** was obtained from mRNA-sequencing of MDA-MB-231 cell line treated with DOC or CAR for 72h). **h-j)** Western blot analysis of active- (non-phosphorylated) β-catenin in MDA-MB-231, MDA-MB-468, and PDC-BRC-101 cell lines treated with DOC or CAR for 1, 3, or 6 days. **k-m)** Gene expression levels obtained via RT-qPCR of Wnt-targets (AXIN2 and LGR5) and stem cell markers (SOX2, POU5F1, and NANOG) in MDA-MB-231, MDA-M-468, and PDC-BRC-101 cell lines treated with DOC or CAR for 72h, displayed as relative expression values (relative to housekeeping genes – HK-genes). Multiple t-tests corrected for multiple comparisons using the Holms-Sidak method (n = 3 independent experiments). All data points shown from min. to max. (box and whiskers). p values are indicated as *$p < 0.05$, **$p < 0.01$, ***$p < 0.001$, ***$p < 0.0001$, and ns, not significant.

FIG2

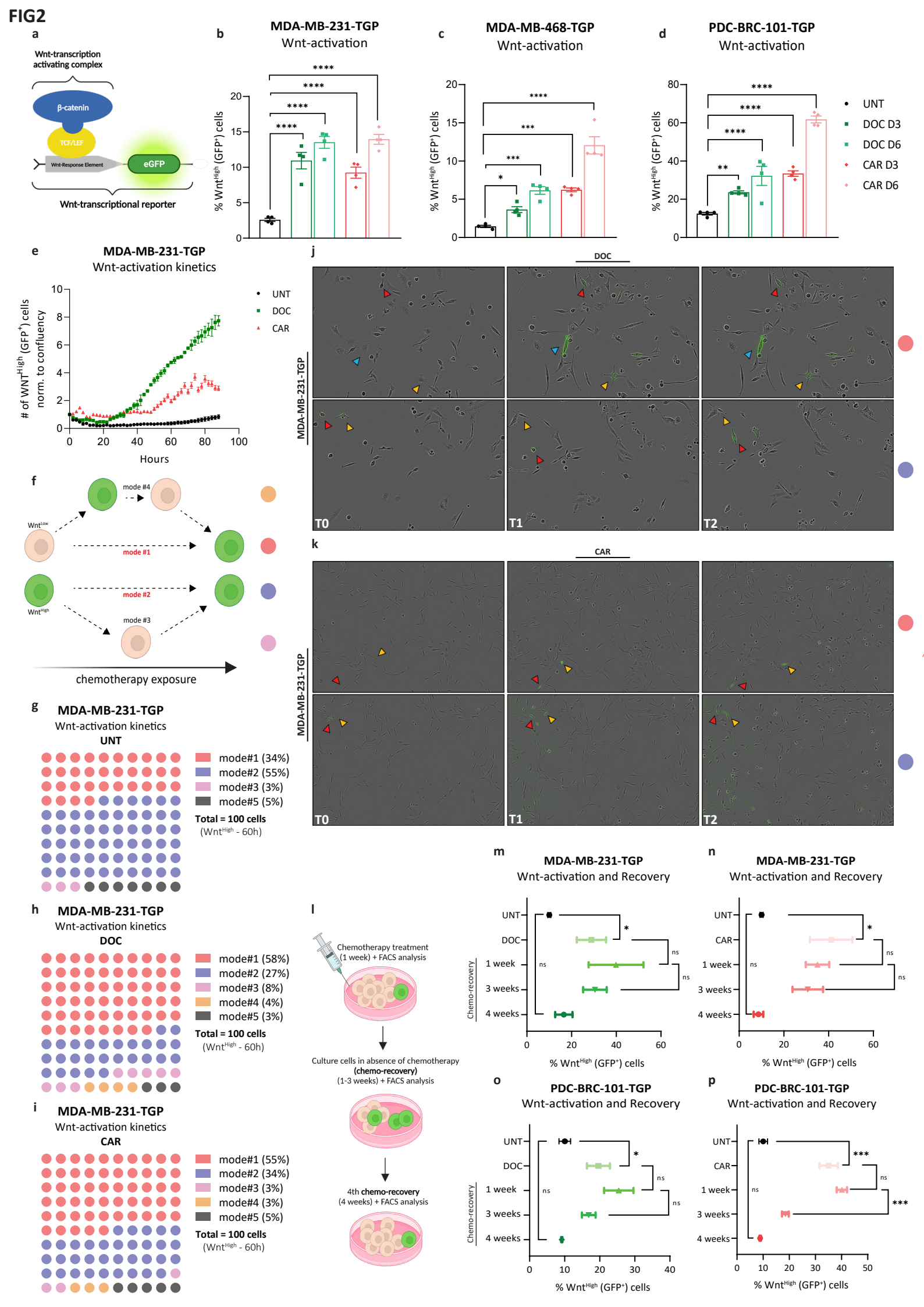
a
Wnt-transcription activating complex
β-catenin
TCF/LEF
Wnt-Response Element
eGFP
Wnt-transcriptional reporter
b
MDA-MB-231-TGP
Wnt-activation
% WntHigh (GFP+) cells
c
MDA-MB-468-TGP
Wnt-activation
d
PDC-BRC-101-TGP
Wnt-activation
UNT
DOC D3
DOC D6
CAR D3
CAR D6
e
MDA-MB-231-TGP
Wnt-activation kinetics
# of WNTHigh (GFP+) cells norm. to confluency
Hours
UNT
DOC
CAR
f
mode #4
WntLow
mode #1
mode #2
WntHigh
mode #3
chemotherapy exposure
g
MDA-MB-231-TGP
Wnt-activation kinetics
UNT
mode#1 (34%)
mode#2 (55%)
mode#3 (3%)
mode#5 (5%)
Total = 100 cells
(WntHigh - 60h)
h
MDA-MB-231-TGP
Wnt-activation kinetics
DOC
mode#1 (58%)
mode#2 (27%)
mode#3 (8%)
mode#4 (4%)
mode#5 (3%)
Total = 100 cells
(WntHigh - 60h)
i
MDA-MB-231-TGP
Wnt-activation kinetics
CAR
mode#1 (55%)
mode#2 (34%)
mode#3 (3%)
mode#4 (3%)
mode#5 (5%)
Total = 100 cells
(WntHigh - 60h)
j
DOC
MDA-MB-231-TGP
T0
T1
T2
k
CAR
MDA-MB-231-TGP
T0
T1
T2
l
Chemotherapy treatment
(1 week) + FACS analysis
Culture cells in absence of chemotherapy
(chemo-recovery)
(1-3 weeks) + FACS analysis
4th chemo-recovery
(4 weeks) + FACS analysis
m
MDA-MB-231-TGP
Wnt-activation and Recovery
UNT
DOC
1 week
3 weeks
4 weeks
Chemo-recovery
% WntHigh (GFP+) cells
n
MDA-MB-231-TGP
Wnt-activation and Recovery
UNT
CAR
1 week
3 weeks
4 weeks
% WntHigh (GFP+) cells
o
PDC-BRC-101-TGP
Wnt-activation and Recovery
UNT
DOC
1 week
3 weeks
4 weeks
Chemo-recovery
% WntHigh (GFP+) cells
p
PDC-BRC-101-TGP
Wnt-activation and Recovery
UNT
CAR
1 week
3 weeks
4 weeks
% WntHigh (GFP+) cells

Figure 2: Induction of transient *de novo* Wnt signaling transcriptional activation in response to chemotherapy in TNBC cell lines

a) Schematic representation of Wnt/β-catenin-transcriptional reporter (TOPGFP). **b-d)** Flow Cytometry analysis displaying % of Wnt^{High} (GFP^{+}) cells for MDA-MB-231-TGP, MDA-MB-468-TGP, and PDC-BRC-101-TGP cell lines treated with DOC or CAR for 3 and 6 days. One-way ANOVA corrected for multiple comparisons using the Holms-Sidak method (n = 4 independent experiments). Data are presented as Mean ± SEM. **e)** Number of Wnt^{High} (GFP^{+}) cells detected by live-cell imaging normalized to the confluency of the well (total number of cells recorded) for MDA-MB-231-TGP cell line treated with DOC or CAR. **f)** Schematic representation of different fluctuation dynamics of Wnt-activation – mode numbered and color coded. **g-i)** Live-imaging quantification of different possible mechanisms of chemotherapy-induced Wnt-activation in MDA-MB-231-TGP TNBC cell line UNT or treated with DOC or CAR. n = 100 cells tracked every 2h for 60h, per treatment condition. Every single cell tracked is represented as a circle and color coded with the scheme shown in **f**. **j-k)** Snapshots of still-frames from time-lapse live imaging experiments of MDA-MB-231-TGP TNBC cell line treated with DOC (top) or CAR (bottom) presenting mode #1 and mode #2 (color coding in scheme shown in f. T_0 indicates 0h, T_1 indicates 30h, and T_2 indicates approx. 50h. Yellow, red, and blue arrows indicate the same cell followed over the treatment period spanning different images (horizontal). **l)** Schematic representation of the experimental setup for chemotherapy treatment and recovery. **m-p)** Flow Cytometry analysis displaying % of Wnt^{High} (GFP^{+}) cells for MDA-MB-231-TGP and PDC-BRC-101-TGP cell lines treated with DOC or CAR for 1 week followed by removal of chemotherapy for 1-, 3-, and 4-weeks post-recovery. Two-tailed unpaired t-test (n=3 independent experiments). Data are presented as Mean ± SEM. p values are indicated as *$p < 0.05$, **$p < 0.01$, ***$p < 0.001$, ****$p < 0.0001$, and ns, not significant.

FIG3

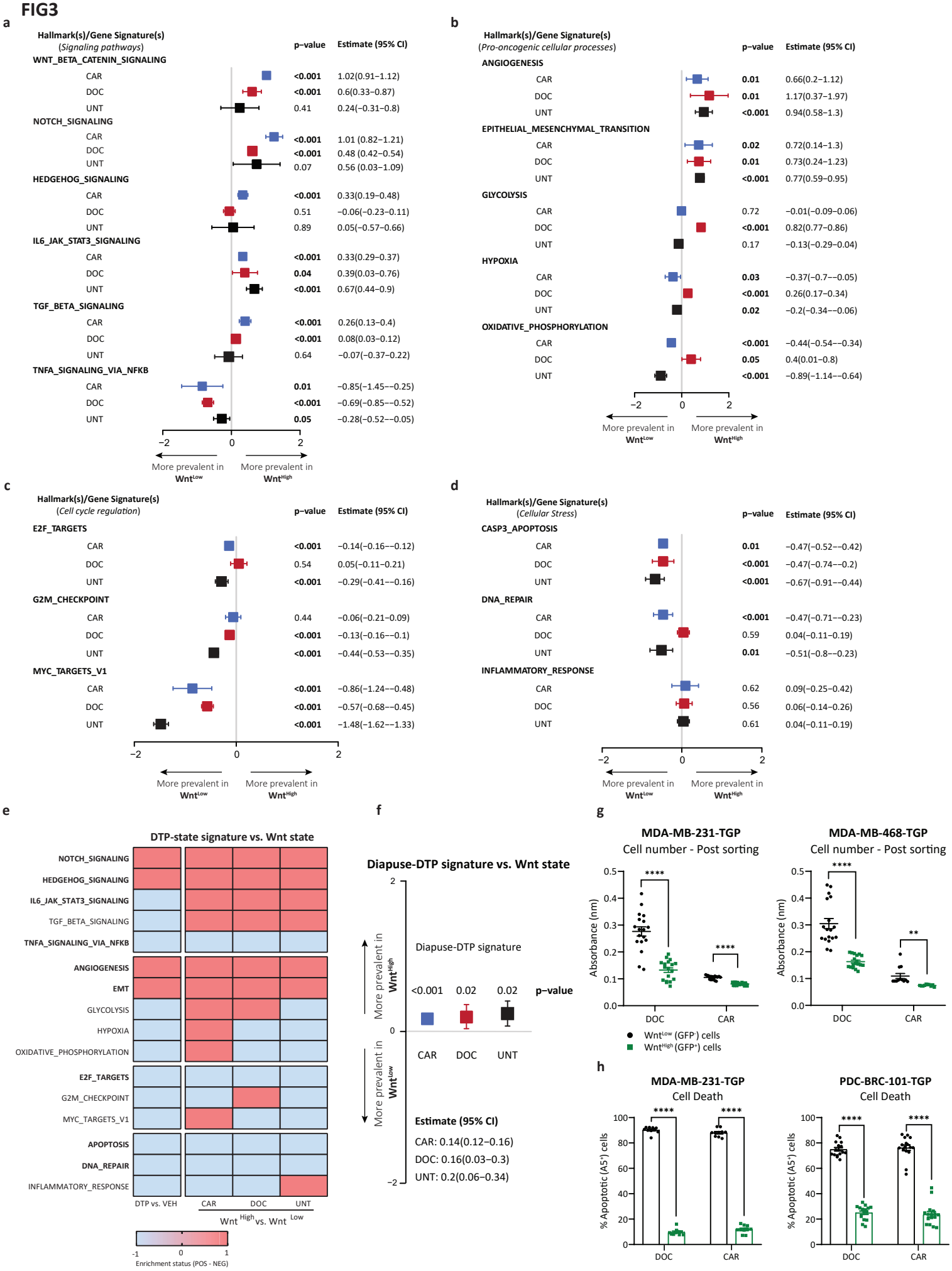
a
Hallmark(s)/Gene Signature(s)
(Signaling pathways)
p–value
Estimate (95% CI)
WNT_BETA_CATENIN_SIGNALING
CAR <0.001 1.02(0.91–1.12)
DOC <0.001 0.6(0.33–0.87)
UNT 0.41 0.24(–0.31–0.8)
NOTCH_SIGNALING
CAR <0.001 1.01 (0.82–1.21)
DOC <0.001 0.48 (0.42–0.54)
UNT 0.07 0.56 (0.03–1.09)
HEDGEHOG_SIGNALING
CAR <0.001 0.33(0.19–0.48)
DOC 0.51 –0.06(–0.23–0.11)
UNT 0.89 0.05(–0.57–0.66)
IL6_JAK_STAT3_SIGNALING
CAR <0.001 0.33(0.29–0.37)
DOC 0.04 0.39(0.03–0.76)
UNT <0.001 0.67(0.44–0.9)
TGF_BETA_SIGNALING
CAR <0.001 0.26(0.13–0.4)
DOC <0.001 0.08(0.03–0.12)
UNT 0.64 –0.07(–0.37–0.22)
TNFA_SIGNALING_VIA_NFKB
CAR 0.01 –0.85(–1.45–-0.25)
DOC <0.001 –0.69(–0.85–-0.52)
UNT 0.05 –0.28(–0.52–-0.05)
–2 0 2
More prevalent in Wnt^Low
More prevalent in Wnt^High
b
Hallmark(s)/Gene Signature(s)
(Pro-oncogenic cellular processes)
p–value
Estimate (95% CI)
ANGIOGENESIS
CAR 0.01 0.66(0.2–1.12)
DOC 0.01 1.17(0.37–1.97)
UNT <0.001 0.94(0.58–1.3)
EPITHELIAL_MESENCHYMAL_TRANSITION
CAR 0.02 0.72(0.14–1.3)
DOC 0.01 0.73(0.24–1.23)
UNT <0.001 0.77(0.59–0.95)
GLYCOLYSIS
CAR 0.72 –0.01(–0.09–0.06)
DOC <0.001 0.82(0.77–0.86)
UNT 0.17 –0.13(–0.29–0.04)
HYPOXIA
CAR 0.03 –0.37(–0.7–-0.05)
DOC <0.001 0.26(0.17–0.34)
UNT 0.02 –0.2(–0.34–-0.06)
OXIDATIVE_PHOSPHORYLATION
CAR <0.001 –0.44(–0.54–-0.34)
DOC 0.05 0.4(0.01–0.8)
UNT <0.001 –0.89(–1.14–-0.64)
–2 0 2
More prevalent in Wnt^Low
More prevalent in Wnt^High
c
Hallmark(s)/Gene Signature(s)
(Cell cycle regulation)
p–value
Estimate (95% CI)
E2F_TARGETS
CAR <0.001 –0.14(–0.16–-0.12)
DOC 0.54 0.05(–0.11–0.21)
UNT <0.001 –0.29(–0.41–-0.16)
G2M_CHECKPOINT
CAR 0.44 –0.06(–0.21–0.09)
DOC <0.001 –0.13(–0.16–-0.1)
UNT <0.001 –0.44(–0.53–-0.35)
MYC_TARGETS_V1
CAR <0.001 –0.86(–1.24–-0.48)
DOC <0.001 –0.57(–0.68–-0.45)
UNT <0.001 –1.48(–1.62–-1.33)
–2 0 2
More prevalent in Wnt^Low
More prevalent in Wnt^High
d
Hallmark(s)/Gene Signature(s)
(Cellular Stress)
p–value
Estimate (95% CI)
CASP3_APOPTOSIS
CAR 0.01 –0.47(–0.52–-0.42)
DOC <0.001 –0.47(–0.74–-0.2)
UNT <0.001 –0.67(–0.91–-0.44)
DNA_REPAIR
CAR <0.001 –0.47(–0.71–-0.23)
DOC 0.59 0.04(–0.11–0.19)
UNT 0.01 –0.51(–0.8–-0.23)
INFLAMMATORY_RESPONSE
CAR 0.62 0.09(–0.25–0.42)
DOC 0.56 0.06(–0.14–0.26)
UNT 0.61 0.04(–0.11–0.19)
–2 0 2
More prevalent in Wnt^Low
More prevalent in Wnt^High
e
DTP-state signature vs. Wnt state
NOTCH_SIGNALING
HEDGEHOG_SIGNALING
IL6_JAK_STAT3_SIGNALING
TGF_BETA_SIGNALING
TNFA_SIGNALING_VIA_NFKB
ANGIOGENESIS
EMT
GLYCOLYSIS
HYPOXIA
OXIDATIVE_PHOSPHORYLATION
E2F_TARGETS
G2M_CHECKPOINT
MYC_TARGETS_V1
APOPTOSIS
DNA_REPAIR
INFLAMMATORY_RESPONSE
DTP vs. VEH
CAR
DOC
UNT
Wnt High vs. Wnt Low
-1 0 1
Enrichment status (POS - NEG)
f
Diapuse-DTP signature vs. Wnt state
2
0
–2
More prevalent in Wnt^High
More prevalent in Wnt^Low
Diapuse-DTP signature
<0.001 0.02 0.02 p–value
CAR DOC UNT
Estimate (95% CI)
CAR: 0.14(0.12–0.16)
DOC: 0.16(0.03–0.3)
UNT: 0.2(0.06–0.34)
g
MDA-MB-231-TGP
Cell number - Post sorting
MDA-MB-468-TGP
Cell number - Post sorting
Absorbance (nm)
0.0 0.1 0.2 0.3 0.4 0.5
****
****
**
DOC
CAR
Wnt^Low (GFP⁻) cells
Wnt^High (GFP⁺) cells
h
MDA-MB-231-TGP
Cell Death
PDC-BRC-101-TGP
Cell Death
% Apoptotic (A5⁺) cells
0 20 40 60 80 100
****
DOC
CAR

Figure 3: Bulk mRNA-sequencing of transcriptionally differential Wnt-populations reveals that chemotherapy-treated Wnt^{High} cells display DTP cell-properties

a-d) Forest plots depicting the association between gene signatures and Wnt-status of sorted Wnt^{High} vs. Wnt^{Low} obtained from samples treated with CAR or DOC or UNT samples. Gene signatures consist of in-house gene signatures[77] and Hallmark gene sets from MSigDB analysed using Gene set variation analysis (GSVA). Quantile regression was used to observe the median change in rescaled gene signatures after accounting for batch effects. Signatures having a non-zero positive estimate indicate increased activity in Wnt^{High} cells. **e)** Correlation analysis between transcriptional DTP cells[9] and Wnt-status of sorted Wnt^{High} vs. Wnt^{Low} cells obtained from samples treated with CAR or DOC and UNT samples. Enrichment status score of -1 (light blue) indicates that a given hallmark/process is downregulated in DTPs or sorted Wnt^{High} cells while a score of 1 (red) indicates that a given hallmark/process is upregulated in DTPs or sorted Wnt^{High} cells. **f)** Forest plot depicting the association between a Diapause-DTP signature[9] and Wnt-status of sorted Wnt^{High} vs. Wnt^{Low} cells obtained from samples treated with CAR or DOC and UNT samples. Analysis performed as in **a-d**. **g)** Absorbance values displaying cellular metabolic activity indicating cell number in sorted MDA-MB-231-TGP and MDA-MB-468-TGP cell lines 1 week after sorting (initial treatment before sorting was with DOC or CAR – 72h). Multiple t-tests corrected for multiple comparisons using the Holms-Sidak method (n = 3 independent experiments). Data are presented as Mean ± SEM. **h)** Flow cytometry analysis displaying % of Apoptotic (Annexin V^+) and their respective Wnt-status (% of Wnt^{High} (GFP^+) cells) of MDA-MB-231-TGP and PDC-BRC-101-TGP cell lines treated with DOC or CAR for 96h. Multiple t-tests corrected for multiple comparisons using the Holms-Sidak method (n = 5 independent experiments). Data are presented as Mean ± SEM. p values are indicated as *$p < 0.05$, **$p < 0.01$, ***$p < 0.001$, ****$p < 0.0001$, and ns, not significant.

FIG4

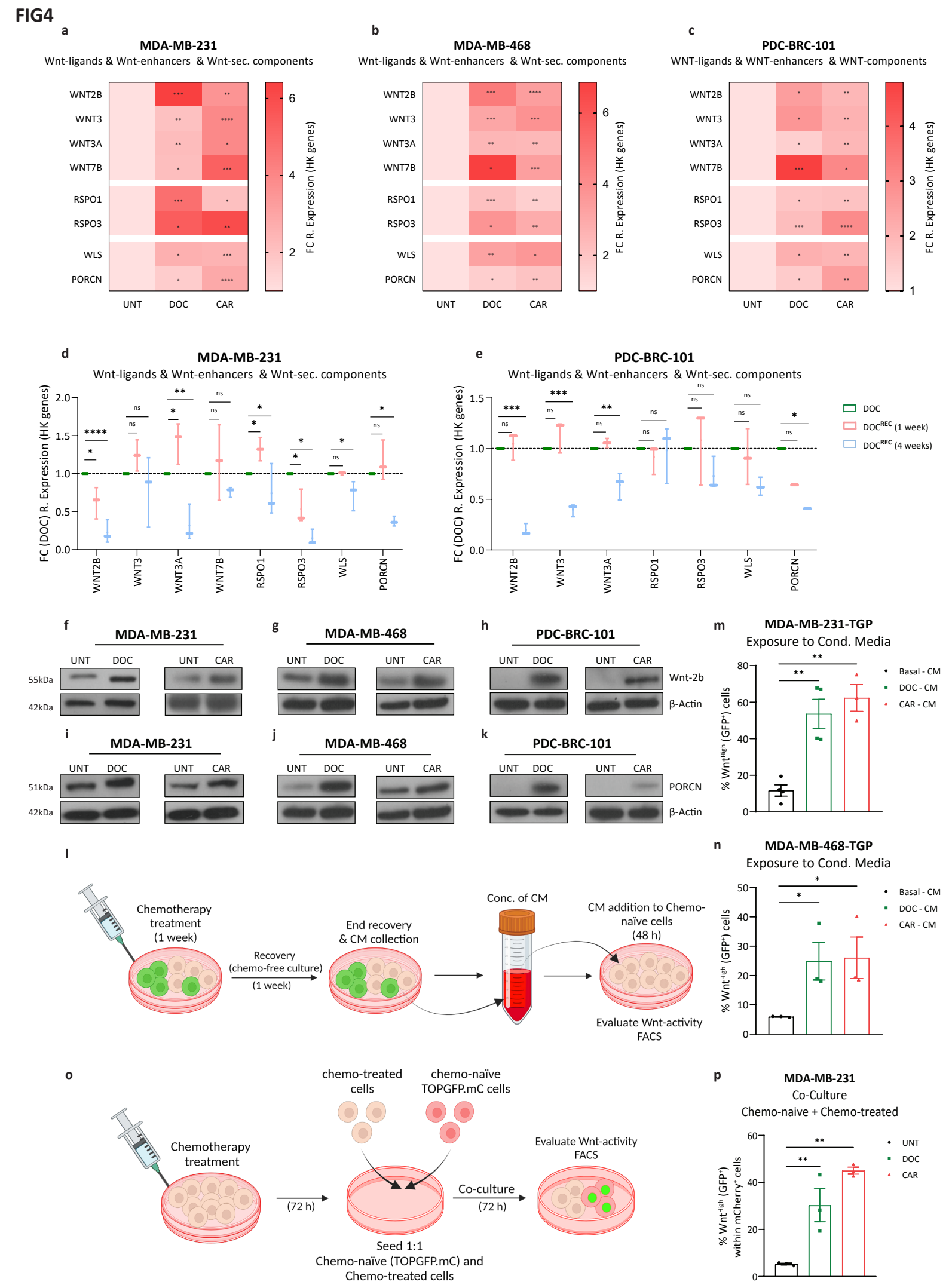
a
MDA-MB-231
Wnt-ligands & Wnt-enhancers & Wnt-sec. components
WNT2B
WNT3
WNT3A
WNT7B
RSPO1
RSPO3
WLS
PORCN
UNT
DOC
CAR
FC R. Expression (HK genes)
b
MDA-MB-468
Wnt-ligands & Wnt-enhancers & Wnt-sec. components
c
PDC-BRC-101
WNT-ligands & WNT-enhancers & WNT-components
d
MDA-MB-231
Wnt-ligands & Wnt-enhancers & Wnt-sec. components
FC (DOC) R. Expression (HK genes)
e
PDC-BRC-101
Wnt-ligands & Wnt-enhancers & Wnt-sec. components
DOC
DOC^REC (1 week)
DOC^REC (4 weeks)
f
MDA-MB-231
g
MDA-MB-468
h
PDC-BRC-101
55kDa
42kDa
Wnt-2b
β-Actin
i
MDA-MB-231
j
MDA-MB-468
k
PDC-BRC-101
51kDa
PORCN
m
MDA-MB-231-TGP
Exposure to Cond. Media
% Wnt^High (GFP+) cells
Basal - CM
DOC - CM
CAR - CM
n
MDA-MB-468-TGP
Exposure to Cond. Media
l
Chemotherapy treatment (1 week)
Recovery (chemo-free culture) (1 week)
End recovery & CM collection
Conc. of CM
CM addition to Chemo-naïve cells (48 h)
Evaluate Wnt-activity FACS
o
Chemotherapy treatment
(72 h)
chemo-treated cells
chemo-naïve TOPGFP.mC cells
Seed 1:1
Chemo-naïve (TOPGFP.mC) and Chemo-treated cells
Co-culture
(72 h)
Evaluate Wnt-activity FACS
p
MDA-MB-231
Co-Culture
Chemo-naive + Chemo-treated
% Wnt^High (GFP+) within mCherry+ cells
UNT
DOC
CAR

Figure 4: Chemotherapeutic treatment induces elevated transcriptional expression of Wnt ligands, Wnt enhancers, and Wnt secretion machinery components

a-c) Heatmaps showing gene expression levels obtained via RT-qPCR of Wnt ligands (WNT2B, WNT3, WNT3A and WNT7B), Wnt enhancers (RSPO1 and RSPO3), and Wnt ligand secretion machinery components (WLS and PORCN) for MDA-MB-231, MDA-MB-468, and PDC-BRC-101 cell lines treated with DOC or CAR for 72h, displayed as fold change (to UNT) of 2^{-dCt} values (relative to HK-genes). Unpaired t-tests based on relative expression values (2^{-dCt}) (n = 3 independent experiments). **d-e)** Gene expression levels as in **a-c** for MDA-MB-231 and PDC-BRC-101 cell lines treated with DOC following the treatment scheme shown in **Fig. 2i**., displayed as fold change (to DOC) of 2^{-dCt} values (relative to HK-genes). Unpaired t-tests based on relative expression values (2dCt) (n = 3 independent experiments). Data are presented as Mean ± SEM. **f-h)** Western blot analysis of Wnt ligand Wnt-2b in MDA-MB-231, MDA-MB-468, and PDC-BRC-101 cell lines treated with DOC or CAR for 72h. **i-k)** Western blot analysis of PORCN in TNBC cell lines treated with DOC or CAR for 72h. **l)** Schematic representation of Conditioned Media (CM) experimental setup. **m-n)** Flow Cytometry analysis displaying % of Wnt^{High} (GFP^{+}) cells of MDA-MB-231-TGP and MDA-MB-468-TGP cell lines cultured with concentrated Basal-, DOC-, or CAR-CM for 48h. Unpaired t-tests (n = 3 independent experiments). Data are presented as Mean ± SEM. **o)** Schematic representation of Co-culture experiment setup. **p)** Flow Cytometry analysis displaying % of Wnt^{High} (GFP^{+}) cells of chemo-naïve MDA-MB-231-TGP.mC co-cultured with chemo-treated DOC or CAR MDA-MB-231 cells for 72h. Unpaired t-tests (n = 3 independent experiments). Data are presented as Mean ± SEM. p values are indicated as *$p < 0.05$, **$p < 0.01$, ***$p < 0.001$, ****$p < 0.0001$, and ns, not significant.

FIG5

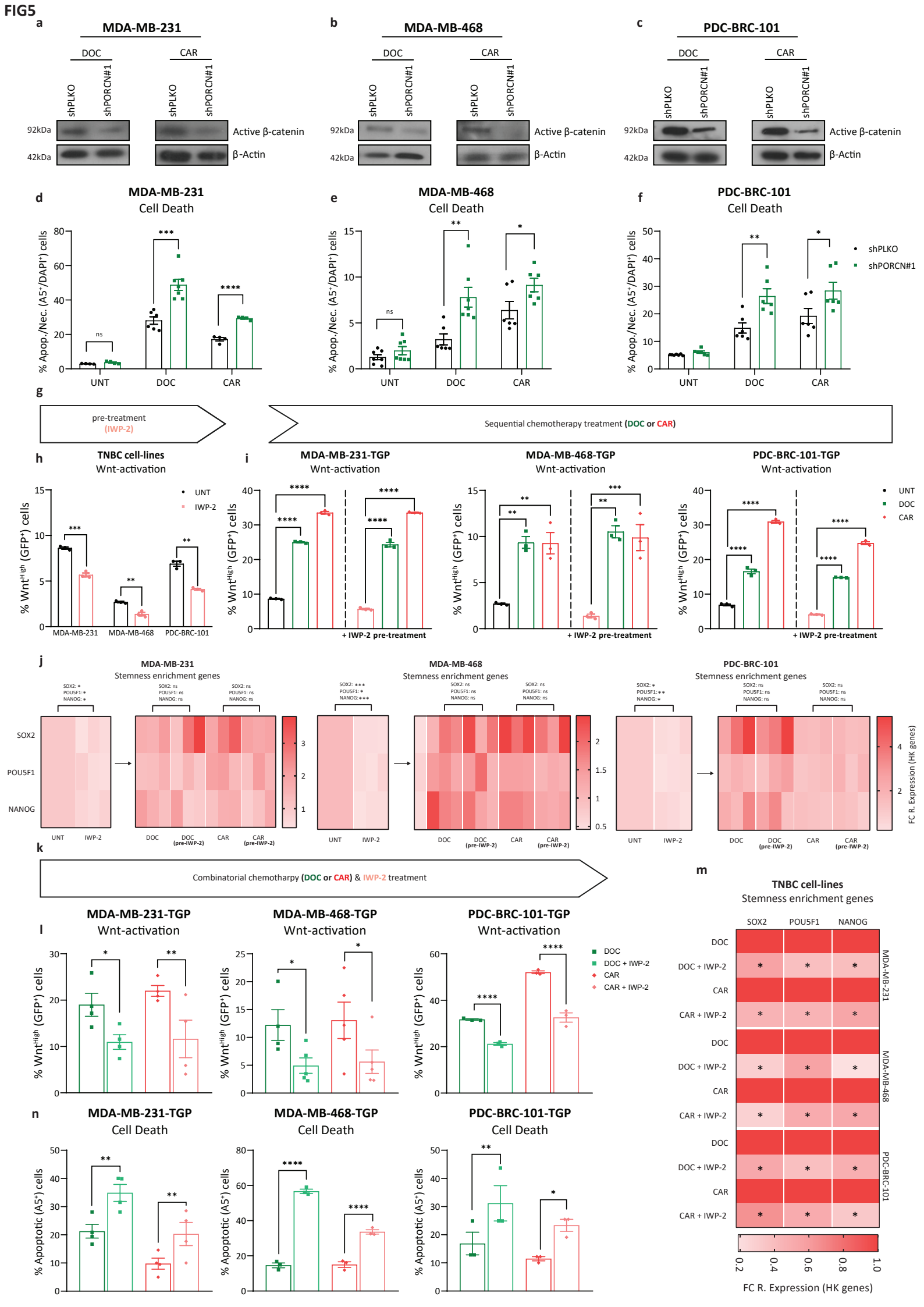
a
MDA-MB-231
DOC
CAR
shPLKO
shPORCN#1
92kDa
42kDa
Active β-catenin
β-Actin
b
MDA-MB-468
c
PDC-BRC-101
d
MDA-MB-231
Cell Death
% Apop./Nec. (A5+/DAPI+) cells
UNT
DOC
CAR
ns
e
MDA-MB-468
Cell Death
f
PDC-BRC-101
Cell Death
shPLKO
shPORCN#1
g
pre-treatment
(IWP-2)
Sequential chemotherapy treatment (DOC or CAR)
h
TNBC cell-lines
Wnt-activation
% WntHigh (GFP+) cells
UNT
IWP-2
MDA-MB-231
MDA-MB-468
PDC-BRC-101
i
MDA-MB-231-TGP
Wnt-activation
MDA-MB-468-TGP
Wnt-activation
PDC-BRC-101-TGP
Wnt-activation
+ IWP-2 pre-treatment
j
MDA-MB-231
Stemness enrichment genes
MDA-MB-468
Stemness enrichment genes
PDC-BRC-101
Stemness enrichment genes
SOX2
POU5F1
NANOG
DOC
DOC (pre-IWP-2)
CAR
CAR (pre-IWP-2)
FC R. Expression (HK genes)
k
Combinatorial chemotharpy (DOC or CAR) & IWP-2 treatment
l
MDA-MB-231-TGP
Wnt-activation
MDA-MB-468-TGP
Wnt-activation
PDC-BRC-101-TGP
Wnt-activation
DOC
DOC + IWP-2
CAR
CAR + IWP-2
m
TNBC cell-lines
Stemness enrichment genes
SOX2
POU5F1
NANOG
MDA-MB-231
MDA-MB-468
PDC-BRC-101
FC R. Expression (HK genes)
n
MDA-MB-231-TGP
Cell Death
MDA-MB-468-TGP
Cell Death
PDC-BRC-101-TGP
Cell Death
% Apoptotic (A5+) cells

Figure 5: Concomitant inhibition of Wnt ligand secretion enhances chemotherapeutic sensitivity in TNBC

a-c) Western blot analysis of active- (non-phosphorylated) β-catenin in MDA-MB-231, MDA-MB-468, and PDC-BRC-101 (shPLKO vs. shPORCN#1) cell lines treated with DOC or CAR for 96h. **d-f)** Flow cytometry analysis displaying % Annexin V^+/$DAPI^+$ cells of MDA-MB-231, MDA-MB-468, and PDC-BRC-101 (shPLKO vs. shPORCN#1) cell lines treated with DOC or CAR for 96h. Unpaired t-tests (n = 4 independent experiments). Data are presented as Mean ± SEM. **g)** Schematic representation of the Sequential Treatment (first IWP-2 pre-treatment followed by chemotherapy) model. **h)** Flow cytometry analysis displaying % of Wnt^{High} (GFP^+) cells of MDA-MB-231-TGP, MDA-MB-468-TGP, and PDC-BRC-101-TGP cell lines pre-treated with IWP-2 (10uM) for 48h. **i)** Flow cytometry analysis of displaying % of Wnt^{High} (GFP^+) cells of TNBC-TGP cell lines treated with DOC or CAR for 72h (with or without IWP-2 pre-treatment). Multiple t-tests corrected for multiple comparisons using the Holms-Sidak method (n = 3 independent experiments). Data are presented as Mean ± SEM. **j)** Heatmaps showing gene expression levels obtained via RT-qPCR of stem cell markers for TNBC cell lines treated with DOC or CAR for 72h (with or without IWP-2 pre-treatment), displayed as fold change (to UNT) of 2^{-dCt} values (relative to HK-genes). Multiple t-tests corrected for multiple comparisons using the Holms-Sidak method based on relative expression values (2^{-dCt}) (n = 3 independent experiments). **k)** Schematic representation of the Combinatorial Treatment model. **l)** Flow cytometry analysis displaying % of Wnt^{High} (GFP^+) cells of TNBC-TGP cell lines treated with DOC or CAR for 96h (sole or in combination with IWP-2). Unpaired t-tests (n = 4 independent experiments). Data are presented as Mean ± SEM. **m)** Heatmaps showing gene expression levels obtained via RT-qPCR of pluripotent stem cell markers for TNBC cell lines treated with DOC or CAR for 96h (sole or in combination with IWP-2), displayed as fold change (to sole treatment) of 2^{-dCt} values (relative to HK-genes). Unpaired t-tests between (DOC vs. DOC + IWP-2 and CAR vs. CAR + IWP-2, for every gene in every cell line) based on relative expression values (2^{-dCt}) (n = 3 independent experiments). **n)** Flow cytometry analysis displaying % of Annexin V^+ cells of TNBC cell lines treated with DOC or CAR for 96h (sole or in combination with IWP-2). Unpaired t-tests (n = 4 independent experiments). Data are presented as Mean ± SEM. p values are indicated as *$p < 0.05$, **$p < 0.01$, ***$p < 0.001$, ****$p < 0.0001$, and ns, not significant.

FIG6

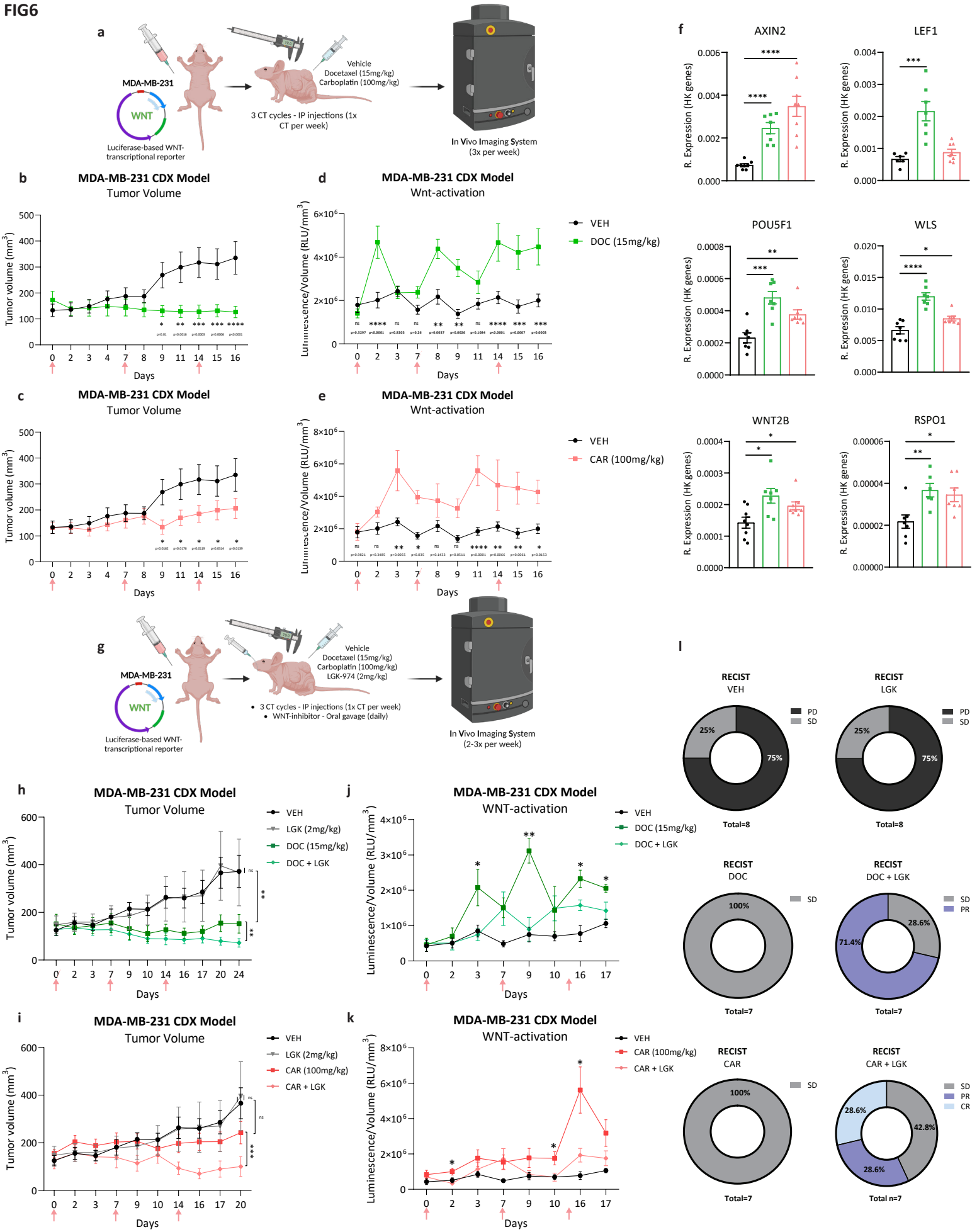
a
MDA-MB-231
WNT
Luciferase-based WNT-transcriptional reporter
Vehicle
Docetaxel (15mg/kg)
Carboplatin (100mg/kg)
3 CT cycles - IP injections (1x CT per week)
In Vivo Imaging System (3x per week)
b
MDA-MB-231 CDX Model
Tumor Volume
Tumor volume (mm3)
Days
c
MDA-MB-231 CDX Model
Tumor Volume
d
MDA-MB-231 CDX Model
Wnt-activation
Luminescence/Volume (RLU/mm3)
VEH
DOC (15mg/kg)
e
MDA-MB-231 CDX Model
Wnt-activation
CAR (100mg/kg)
f
AXIN2
LEF1
POU5F1
WLS
WNT2B
RSPO1
R. Expression (HK genes)
g
Vehicle
Docetaxel (15mg/kg)
Carboplatin (100mg/kg)
LGK-974 (2mg/kg)
3 CT cycles - IP injections (1x CT per week)
WNT-inhibitor - Oral gavage (daily)
In Vivo Imaging System (2-3x per week)
h
MDA-MB-231 CDX Model
Tumor Volume
VEH
LGK (2mg/kg)
DOC (15mg/kg)
DOC + LGK
j
MDA-MB-231 CDX Model
WNT-activation
i
MDA-MB-231 CDX Model
Tumor Volume
CAR (100mg/kg)
CAR + LGK
k
MDA-MB-231 CDX Model
WNT-activation
l
RECIST VEH
RECIST LGK
RECIST DOC
RECIST DOC + LGK
RECIST CAR
RECIST CAR + LGK
PD
SD
PR
CR
Total=8
Total=7
Total n=7

Figure 6: Inhibition of Wnt ligand secretion and chemotherapeutic treatment synergistically sensitize *in vivo* xenograft TNBC model to treatment

a) Schematic representation of cell line derived xenograft (CDX) experimental setup to study Wnt signaling pathway kinetics upon chemotherapeutic treatment *in vivo*. **b-c)** Tumor growth curves of subcutaneous generated xenograft models treated with VEH, DOC (15mg/kg/week – top), or CAR (100mg/kg/week – bottom). Pink arrows indicate administration of chemotherapy. Two-way ANOVA with Fisher's LSD test (n = 7 mice for all treatment groups). Data are presented as Mean ± SEM. **d-e)** Levels of Wnt-activation (RLU/mm³) displayed as luminescent signals (RLU) captured by IVIS Spectrum normalized to tumor volume (mm³) in xenograft models treated with VEH, DOC (top), or CAR (bottom). Two-way ANOVA with Fisher's LSD test (n = 7 mice for all treatment groups). Data are presented as Mean ± SEM. **f)** Gene expression levels obtained via RT-qPCR of various Wnt-targets, stem cell markers, and Wnt-activators in samples resected from xenograft models treated with VEH, DOC, or CAR. Unpaired t-tests based on relative expression values (2^{-dCt}) (n = 7 mice for all treatment groups). Data are presented as Mean ± SEM. **g)** Schematic representation of CDX experimental setup with Wnt ligand secretion inhibition *in vivo*. **h-i)** Tumor growth curves of xenograft models treated with VEH, LGK (2mg/kg/day), DOC (top), DOC+LGK (top), CAR (bottom), and CAR+LGK (bottom). Pink arrows indicate administration of chemotherapy. Paired t-tests (based on final tumor volumes – obtained on day of sacrifice, n = 8,7,6,5 mice per treatment group). Data are presented as Mean ± SEM. **j-k)** Levels of Wnt-activation (RLU/mm³) displayed as luminescent signals (RLU) captured by IVIS Spectrum normalized to tumor volume (mm³) in xenograft models treated with VEH, DOC (top), DOC+LGK (top), CAR (bottom), and CAR+LGK (bottom). Multiple t-tests (n = 8,7,6,5 mice per treatment group). Data are presented as Mean ± SEM. **l)** RECIST analysis displayed as percentage of animals per treatment group (VEH, LGK, DOC, DOC+LGK, CAR, and CAR+LGK) classified/assigned to one of four distinct tumor responses to treatment: Progressive Disease (PD), Stable Disease (SD), Partial Response (PR), or Complete Response (CR). p values are indicated as *$p < 0.05$, **$p < 0.01$, ***$p < 0.001$, ****$p < 0.0001$, and ns, not significant.

FIG7

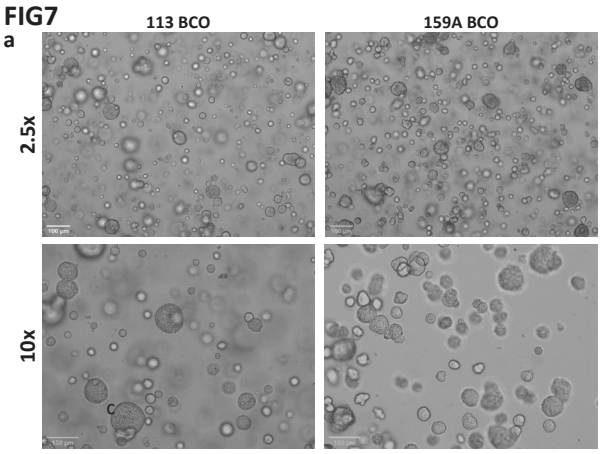
a
113 BCO
159A BCO
2.5x
10x

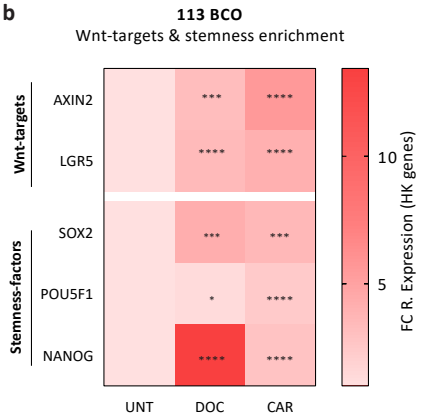
b
113 BCO
Wnt-targets & stemness enrichment
Wnt-targets
Stemness-factors
AXIN2
LGR5
SOX2
POU5F1
NANOG
UNT
DOC
CAR
FC R. Expression (HK genes)

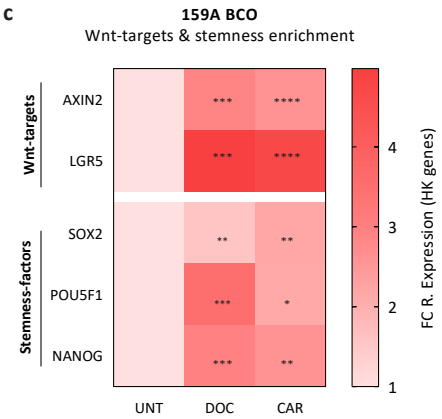
c
159A BCO
Wnt-targets & stemness enrichment
Wnt-targets
Stemness-factors
AXIN2
LGR5
SOX2
POU5F1
NANOG
UNT
DOC
CAR
FC R. Expression (HK genes)

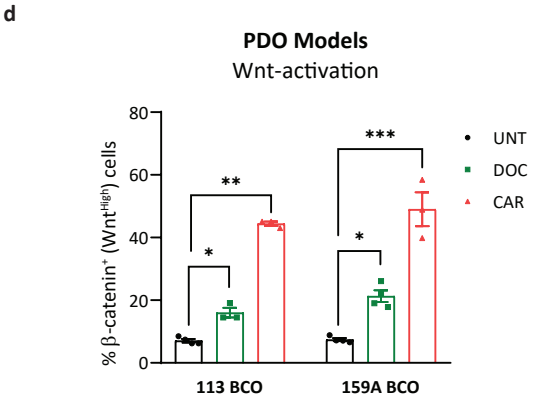
d
PDO Models
Wnt-activation
% β-catenin⁺ (Wnt^High) cells
113 BCO
159A BCO
UNT
DOC
CAR

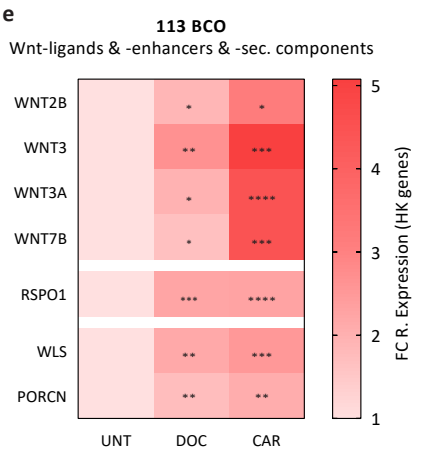
e
113 BCO
Wnt-ligands & -enhancers & -sec. components
WNT2B
WNT3
WNT3A
WNT7B
RSPO1
WLS
PORCN
UNT
DOC
CAR
FC R. Expression (HK genes)

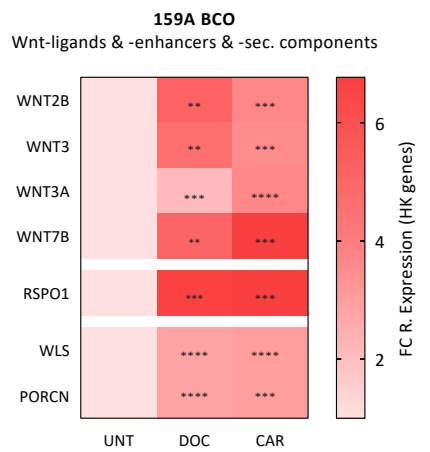
f
159A BCO
Wnt-ligands & -enhancers & -sec. components
WNT2B
WNT3
WNT3A
WNT7B
RSPO1
WLS
PORCN
UNT
DOC
CAR
FC R. Expression (HK genes)

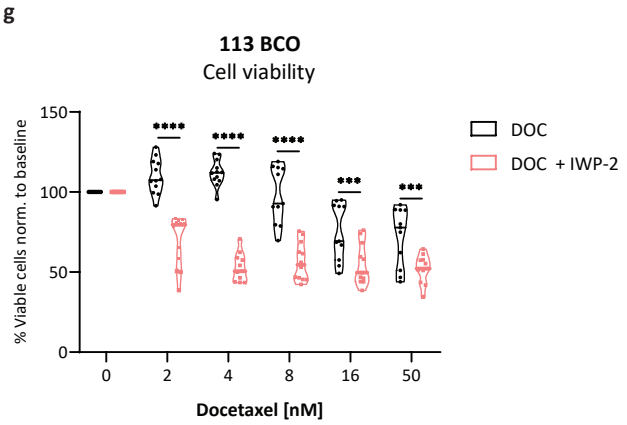
g
113 BCO
Cell viability
% Viable cells norm. to baseline
Docetaxel [nM]
DOC
DOC + IWP-2

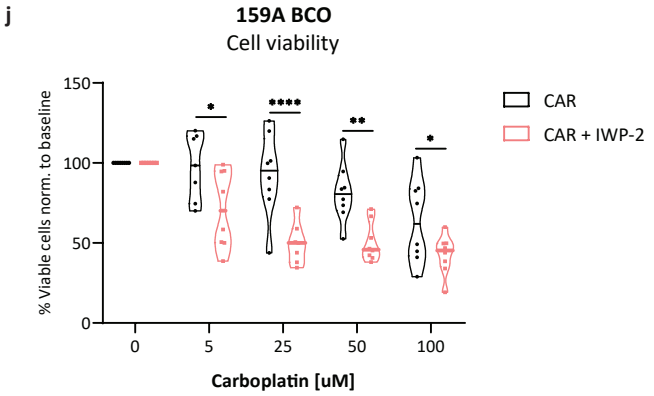
j
159A BCO
Cell viability
% Viable cells norm. to baseline
Carboplatin [uM]
CAR
CAR + IWP-2

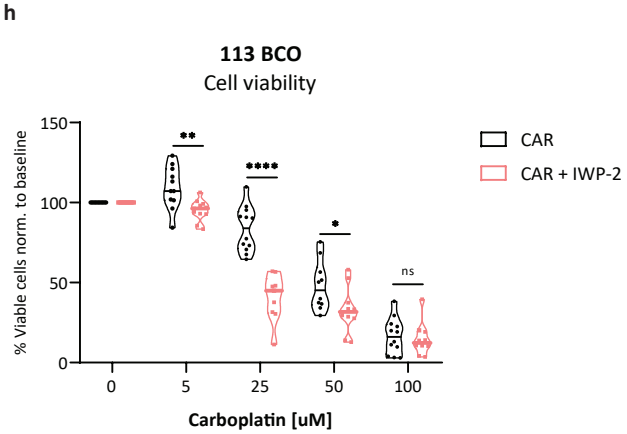
h
113 BCO
Cell viability
% Viable cells norm. to baseline
Carboplatin [uM]
CAR
CAR + IWP-2

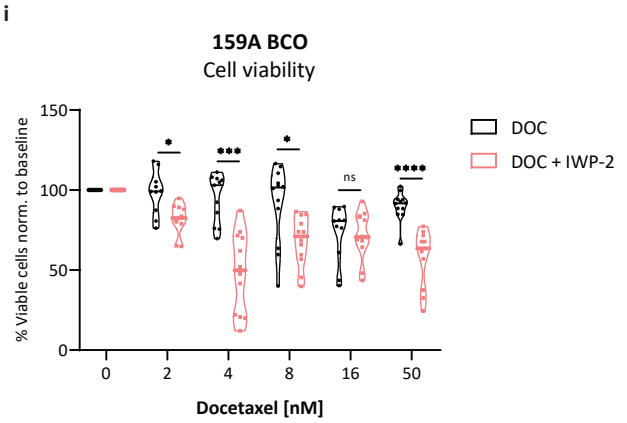
i
159A BCO
Cell viability
% Viable cells norm. to baseline
Docetaxel [nM]
DOC
DOC + IWP-2

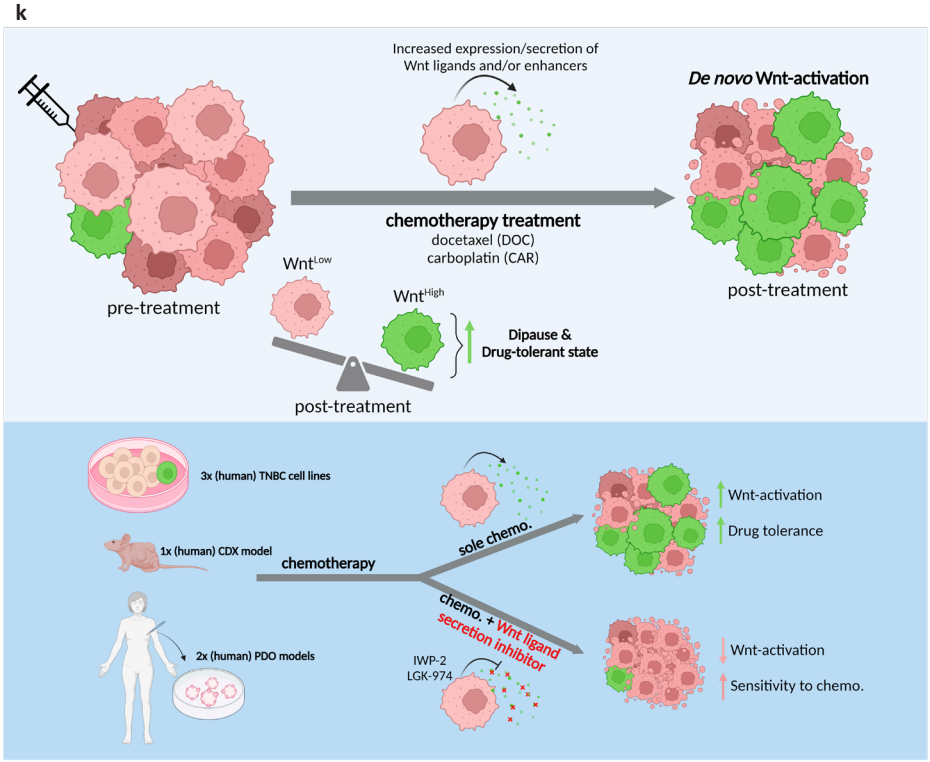
k
Increased expression/secretion of
Wnt ligands and/or enhancers
De novo Wnt-activation
chemotherapy treatment
docetaxel (DOC)
carboplatin (CAR)
pre-treatment
post-treatment
Wnt^Low
Wnt^High
Dipause &
Drug-tolerant state
post-treatment
3x (human) TNBC cell lines
1x (human) CDX model
2x (human) PDO models
chemotherapy
sole chemo.
chemo. + Wnt ligand secretion inhibitor
IWP-2
LGK-974
Wnt-activation
Drug tolerance
Wnt-activation
Sensitivity to chemo.

Figure 7: Preclinical PDO models recapitulate chemotherapy-mediated Wnt-activation and sensitization to synergistic Wnt ligand secretion inhibition

a) Phase-contrast images of TNBC-PDO models, 113 BCO (left) and 159A BCO (right) in basal culture conditions at 2.5x (top) and 10x (bottom) magnification **b-c)** Heatmaps showing gene expression levels obtained via RT-qPCR of Wnt-targets and stem cell markers for 113 BCO and 159A BCO models treated with DOC (16nM for 113 BCO and 8nM for 159A BCO) or CAR (50µM for 113 BCO and 125µM for 159A BCO) for 96h, displayed as fold change (to UNT) of 2^{-dCt} values (relative to HK-genes). Unpaired t-tests based on relative expression values (2dCt) (n = 4 independent experiments). **d)** Flow cytometry analysis displaying % of Wnt-active (β-catenin^{+}) cells from 113 BCO (left) and 159A BCO (right) models treated with DOC or CAR for 96h. Multiple t-tests corrected for multiple comparisons using the Holm-Sidak method (n = 3 independent experiments). Data are presented as Mean ± SEM. **e-f)** Heatmaps showing gene expression levels obtained via RT-qPCR of Wnt-ligands, -enhancers, and -secretion machinery components for 113 BCO (left) and 159A BCO (right) models treated with DOC or CAR for 96h, displayed as fold change (to UNT) of 2^{-dCt} values (relative to HK-genes). Unpaired t-tests based on relative expression values (2^{-dCt}) (n = 4 independent experiments). **g-j)** Drug dose-response curves of 113 BCO (left) and 159A BCO (right) models treated with increasing concentrations of DOC or CAR (sole or in combination with IWP-2, 50uM). Viability in sole- or combinatorial-treatment is normalized to UNT or sole-IWP-2 conditions (baseline). Multiple t-tests corrected for multiple comparisons using the Holm-Sidak method (n = 4 independent experiments). Data are presented as Mean ± SEM. **k)** Graphical illustration representing a schematic summary of key findings and observations. p values are indicated as *$p < 0.05$, **$p < 0.01$, ***$p < 0.001$, ****$p < 0.0001$, and ns, not significant.